Table 3.3.1-1. Mean Annual Precipitation for Analogues for the Lower and Upper Bound of the Three Climate Scenarios Adjusted for the Topography of the UZ Flow and Transport Model Area

Climate	Lower Bound (mm/yr)	Mean (mm/yr)	Upper Bound (mm/yr)
Interglacial[a]	186.8	190.6	268.6
Monsoon[b]	190.6	302.7	414.8
Intermediate[c]	202.2	317.8	433.5

Sources: [a] Adapted from USGS 2001 [DIRS 154674], Table 6-9.
[b] Adapted from USGS 2001 [DIRS 154674], Table 6-13.
[c] Adapted from USGS 2001 [DIRS 154674], Table 6-18.

NOTE: In *Simulation of Net Infiltration for Modern and Potential Future Climates* (USGS 2001 [DIRS 154674]), the interglacial and intermediate climates are referred to as modern and glacial transition, respectively.

Table 3.3.1-2. Mean Annual Temperature for Analogues for the Lower and Upper Bound of the Three Climate Scenarios Adjusted for the Topography of the UZ Flow and Transport Model Area

Climate	Lower Bound (°C)	Mean (°C)	Upper Bound (°C)
Interglacial[a]	19.3	19.3	19.3
Monsoon[b]	17.3	17.2	17.0
Intermediate[c]	10.2	9.8	9.4

Sources: [a] DTN: GS010508311221.001 [DIRS 154998].
[b] Adapted from USGS 2001 [DIRS 154674], Table 6-12.
[c] Adapted from USGS 2001 [DIRS 154674], Table 6-17.

NOTE: Lower and upper refer to precipitation (Table 3.3.1-1), not temperature. In *Simulation of Net Infiltration for Modern and Potential Future Climates* (USGS 2001 [DIRS 154674]), the interglacial and intermediate climates are referred to as modern and glacial transition, respectively.

Table 3.3.1-3. Climate Sequence from 10,000 to 1 Million Years

Climate State	Begin Time (years)	End Time (years)
Intermediate/Monsoon	10,000	38,000
Glacial, Stage 8/10	38,000	49,000
Intermediate	49,000	65,000
Interglacial	65,000	77,000
Intermediate/Monsoon	77,000	106,000
Glacial, Stage 8/10	106,000	120,000
Intermediate	120,000	137,000
Interglacial	137,000	148,000
Intermediate/Monsoon	148,000	200,000
Glacial, Stage 6/16	200,000	213,000
Intermediate	213,000	229,000
Interglacial	229,000	241,000
Intermediate/Monsoon	241,000	291,000
Glacial, Stage 4	291,000	329,000
Intermediate	329,000	345,000
Interglacial	345,000	355,000
Intermediate/Monsoon	355,000	401,000

Table 3.3.1-3. Climate Sequence from 10,000 to 1 Million Years (Continued)

Climate State	Begin Time (years)	End Time (years)
Glacial, Stage 8/10	401,000	409,000
Intermediate	409,000	422,000
Interglacial	422,000	432,000
Intermediate/Monsoon	432,000	471,000
Glacial, Stage 8/10	471,000	482,000
Intermediate	482,000	497,000
Interglacial	497,000	507,000
Intermediate/Monsoon	507,000	555,000
Glacial, Stage 6/16	555,000	595,000
Intermediate	595,000	611,000
Interglacial	611,000	622,000
Intermediate/Monsoon	622,000	672,000
Glacial, Stage 4	672,000	688,000
Intermediate	688,000	704,000
Interglacial	704,000	715,000
Intermediate/Monsoon	715,000	761,000
Glacial, Stage 8/10	761,000	788,000
Intermediate	788,000	801,000
Interglacial	801,000	811,000
Intermediate/Monsoon	811,000	854,000
Glacial, Stage 8/10	854,000	864,000
Intermediate	864,000	877,000
Interglacial	877,000	887,000
Intermediate/Monsoon	887,000	934,000
Glacial, Stage 6/16	934,000	957,000
Intermediate	957,000	970,000
Interglacial	970,000	981,000
Intermediate/Monsoon	981,000	1,000,000

Source: CRWMS M&O 2000 [DIRS 153038], Table 6-6.

Table 3.3.1-4. Summary of Uncertainty Issues Related to the Development of the Climate Model

Category	Uncertainty Issue	Treatment of Uncertainty Issue	Affected Goals
Conceptual Uncertainties	Timing and severity of climate changes during 400,000 year cycle. Past glacial and interglacial climate couplets differ from each other and past climates are repeated in a predetermined order.	Comparison of past records suggests climate cyclicity and the Devils Hole record records a series of glacial/interglacial couplets (CRWMS M&O 2000 [DIRS 153038], Section 6.3). The Owens Lake record is used to describe the climate conditions of the interval selected as the climate analogue. Climate change can be timed with an earth-orbital clock of precession and eccentricity, so the timing of future climate change can be estimated from the orbital clock. Orbital parameters for the earth can be readily calculated and the paleoclimatic record compared to the orbital parameters. Depends on the available record and the interpretation of paleoenvironments from the last 400,000 years. Temperature and precipitation characteristics of past glacial and interglacial couplets can differ from each other in a systematic way through a 400,000 year cycle, and if the sequence of an adjacent cycle is similar, then this relation can provide a criterion for the selection of particular past climates to project into the future.	Infiltration boundary condition for flow and transport models. Estimates of the sequence, magnitude, and timing of future climate states.
	Long-term earth-based climate-forcing functions, such as tectonic change, have remained relatively constant over the past 500,000 years.	Climate should not be greatly affected for the next 500,000 years (first half of the future climate analysis), but Tectonic activities may impact future climate at the 1 million-year time scale. The impact of potential future Tectonic activity was not estimated because it is not present in the Devils Hole and Owens Lake records.	
Data Uncertainties	The paleoecological and paleoclimatic records representative of Yucca Mountain.	Proxy data from the Yucca Mountain regional area are used to estimate past climates at Yucca Mountain.	Estimates of the timing, nature, and sequence of future climate states.
	Secular variation in the tidal dissipation and dynamical ellipticity of the earth.	Uncertainties are within the level of confidence of this methodology.	Estimates on the timing of future climate states.

Table 3.3.1-4. Summary of Uncertainty Issues Related to the Development of the Climate Model (Continued)

Category	Uncertainty Issue	Treatment of Uncertainty issue	Affected Goals
Parameter Uncertainties	Climate impact	Upper and lower bounds for each climate state estimated from what analogue meteorological stations Provide a range to capture the variability of climate	Temperature and precipitation estimates for different climate states
	Timing of future climates	Timing errors estimated are well within the level of confidence appropriate for their intended use	Timing of future climate states
	Methodological uncertainty	This methodology (forecasting) was selected over modeling because modeling requires the input of future boundary conditions which are unknown	Timing and sequence of climate states
	Unanticipated, unknown, and unmeasurable future events such as anthropogenic change, volcanic eruptions, tectonic change, change in solar output, and meteor showers	The most probable effect of anthropogenic change on future climate would be global warming, which would prolong the current interglacial period and delay the onset of future intermediate and glacial climates. This makes the climate modeling less certain, but because those climates are colder and wetter than the present climate, the present TSPA model is conservative for its intended use. Other climate-affecting events are unpredictable.	Estimates of the sequence, magnitude, and timing of future climate states

Table 3.3.1-5. Mean Annual Precipitation for the Lower and Upper Bound of the Three Glacial Climate Scenarios Adjusted for the Topography of the UZ Flow and Transport Model Area

Climate	Lower Bound (mm/yr)	Mean (mm/yr)	Upper Bound (mm/yr)
Glacial, Stage 8/10	433.5[a] (391.0[f])	429.0[c]	529.0[d]
Glacial, Stage 6/16	330.0[b]	429.0[c]	529.0[d]
Glacial, Stage 4	269.0[e]	330.0[b]	429.0[c]

Source: Adapted from BSC 2001 [DIRS 154873].

NOTES: [a] Rosalia, WA; Spokane, WA; St. John, WA (upper-bound intermediate climate meteorological stations).
[b] Browning, MT; Simpson 6NW, MT.
[c] Lake Yellowstone, WY; Browning, MT; Simpson 6NW, MT.
[d] Lake Yellowstone, WY.
[e] Simpson 6NW, MT.
[f] Browning, MT (alternate Stage 6/16 meteorological station).

Table 3.3.1-6. Mean Annual Temperature for the Lower and Upper Bound of the Three Glacial Climate Scenarios Adjusted for the Topography of the UZ Flow and Transport Model Area

Climate	Lower Bound (°C)	Mean (°C)	Upper Bound (°C)
Glacial, Stage 8/10	9.4[a] (5.3[f])	3.1[c]	0.78[d]
Glacial, Stage 6/16	5.5[b]	3.1[c]	0.78[d]
Glacial, Stage 4	5.7[e]	5.5[b]	3.1[c]

Source: Adapted from BSC 2001 [DIRS 154873].

NOTES: [a] Rosalia, WA; Spokane, WA; St. John, WA (upper-bound intermediate climate meteorological stations).
[b] Browning, MT; Simpson 6NW, MT.
[c] Lake Yellowstone, WY; Browning, MT; Simpson 6NW, MT.
[d] Lake Yellowstone, WY.
[e] Simpson 6NW, MT.
[f] Browning, MT (alternate Stage 6/16 meteorological station).

Lower and upper refer to precipitation (Table 3.3.1-5) or net infiltration (Table 3.3.2-3), not temperature.

Table 3.3.2-1. Average Net Infiltration Rates over the Unsaturated Zone Flow and Transport Model Domain for the Modern, Monsoon, and Glacial Transition Climate States

Climate	Lower Bound (mm/yr)	Mean (mm/yr)	Upper Bound (mm/yr)
Interglacial[a]	1.3	4.6	11.1
Monsoon[b]	4.6	12.2	19.8
Intermediate[c]	2.5	17.8	33.0

Sources: [a] Adapted from USGS 2001 [DIRS 154674], Table 6-9.
[b] Adapted from USGS 2001 [DIRS 154674], Table 6-13.
[c] Adapted from USGS 2001 [DIRS 154674], Table 6-18.

NOTE: In *Simulation of Net Infiltration for Modern and Potential Future Climates* (USGS 2001 [DIRS 154674]), the interglacial and intermediate climates are referred to as modern and glacial transition, respectively.

Table 3.3.2-2. Summary of Uncertainty Issues Related to the Development of the Net Infiltration Model

Category	Uncertainty Issue	Treatment of Uncertainty Issue	Affected Goals
Conceptual Uncertainties	The net infiltration model (USGS 2000 [DIRS 139422]) uses a distributed parameter, quasi-three-dimensional water-balance approach for simulating runoff and net infiltration processes without necessarily representing the physics of infiltration in soils and stream flow	The net infiltration model was compared successfully to several independent approaches to estimating net infiltration and recharge (USGS 2001 [DIRS 154674], Section 6.8) The net infiltration model was calibrated using moisture profile, soil and bedrock hydrologic properties, meteorological data and stream flow measurements at Yucca Mountain	Estimates of net infiltration rate resulting from the various different climate states
	The scope of the net infiltration model is limited to surficial hydrologic processes, with estimates of net infiltration limited to vertical flow though the depth of the root zone only	Vertical one-dimensional flow of infiltrating water through the root zone is supported by data (USGS 2001 [DIRS 154674], Section 6.8). Data indicating ponding of water within the root zone or on the soil/bedrock interface from the episodic infiltration events resulting in lateral flow has not been found	Estimates of net infiltration rate resulting from the various different climate states
Data Uncertainties	Precipitation rates and temperatures resulting from future climates	Data obtained from meteorological stations used in the Climate Model are believed to be representative of future climates at Yucca Mountain based upon ostracode populations and geographic similarity, location and proximity to Yucca Mountain	Estimates of net infiltration rate resulting from the various different climate states
	Accuracy of field data used to calibrate the net infiltration model for the modern (present-day) climate state	Extensive data regarding the time series of water-content profiles in boreholes by neutron logging, water potential at the soil/bedrock contact, and stream-flow measurements caused by transient precipitation events were collected	Parameters in the net infiltration model for the modern climate state
Parameter Uncertainties	Root-zone weighting parameters, vegetation density, changes in vegetation type and root zone thickness are a function of the climate state	These parameters were adjusted by a constant factor to extrapolate from present day conditions at Yucca Mountain to those anticipated to occur under future climate states (USGS 2001 [DIRS 154674], Section 6.9)	Estimates of net infiltration rate resulting from the various different climate states
	Uncertainty in net infiltration results from imperfect knowledge of input parameters used by the net infiltration model	A TSPA uncertainty analysis (Section 3.3.2.6) was conducted, focusing on twelve key input parameters for which uncertainty distributions were developed (USGS 2001 [DIRS 154674], Section 6.10.2). The key parameters were: bedrock porosity, bedrock root zone thickness, soil depth, precipitation, potential evapotranspiration, bedrock saturated hydraulic conductivity, soil saturated hydraulic conductivity, two bare-soil evaporation parameters, effective surface-water flow area, and parameters associated with sublimation and melting of snow cover	Estimates of net infiltration rate resulting from the various different climate states

Table 3.3.2-3. Average Net Infiltration Rates over the Unsaturated Zone Flow and Transport Model Domain for Full Glacial Climate States

Climate	Lower Bound (mm/yr)	Mean (mm/yr)	Upper Bound (mm/yr)
Glacial, Stage 8/10	33.0[a] (36.0[b])	87.9	151.0
Glacial, Stage 6/16	24.4	87.9	151.0
Glacial, Stage 4	12.9	24.4	87.9

Source: Adapted from BSC 2001 [DIRS 154919].

NOTES: [a] Derived using upper-bound intermediate climate meteorological station data (Tables 3.3.1-5, 3.3.1-6).
[b] Derived using alternate Stage 6/16 meteorological station data (Tables 3.3.1-5, 3.3.1-6).

Table 3.3.3-1. Net Infiltration Data by Region

Region	Area		Net Infiltration Volume				Net Infiltration Rate	
			Before Calibration		After Calibration		Before Calibration	After Calibration
	km^2	%	m^3/yr	%	m^3/yr	%	mm/yr	mm/yr
I	9.9	25.5	104435	58.9	104436	54.2	10.57	10.57
II	5.3	13.8	12317	6.9	12317	6.4	2.31	2.31
III	3.7	9.6	26266	14.8	20194	10.6	7.10	5.46
IV	3.6	9.4	8819	5.0	16267	8.4	2.43	4.48
V	4.6	11.9	12510	7.1	17534	9.1	2.71	3.80
VI	2.2	5.6	2479	1.4	5447	2.8	1.14	2.51
VII	1.8	4.6	3345	1.9	3345	1.7	1.88	1.88
VIII	3.0	7.7	2156	1.2	2156	1.1	0.73	0.73
IX	4.7	12.0	4996	2.8	11022	5.7	1.07	2.36
Overall	38.7	100.0	177323	100.0	192718	100.0	4.58	4.98

Source: Before calibration DTN: GS000399991221.002 [DIRS 147022]; after calibration Bodvarsson 2001 [DIRS 154669], Attachment 11.

Table 3.3.3-2. Summary of Uncertainty Issues Related to Percolation Redistribution and Flow in PTn

Category	Uncertainty Issue	Treatment of Uncertainty Issue	Affected Goals
Conceptual Uncertainties	Lateral flow at PTn interfaces and in PTn.	Sensitivity simulations to evaluate the impacts of fine tuff layers, lateral discontinuities, upper and side (fault) boundary conditions, fracture, matrix, and fault properties. Multi-scale evaluations for the conceptual basis of heterogeneity representation, multicontinuum approaches, and discrete flow path approaches.	Development of conceptual models is consistent with the geologic, hydrologic, and geochemical observations.
	Role of PTn in damping spatial and temporal variabilities.	Quantify the effectiveness of damping by sensitivity simulations, field data collection, environmental tracer distributions, and controlled field tests.	
	Fast flow through PTn.	Quantify the sustainability of fast flow through heterogeneous units, with strong capillary forces and imbibition potentials by sensitivity simulations, field data collection, water and rock age sampling, and controlled field tests.	
	Transition from porous medium to fracture flow at PTn interfaces.	Quantify transition from porous flow in porous layers to fracture flow in fractured layers by sensitivity simulations, field data collection, and controlled flow tests.	
Data Uncertainties	Uncertainties of data used for calibration and validation of PTn property model.	Systematic collection of water potential, water saturation, saturation characteristic curves, relative permeability curves, chemical contents, isotopic ages, and relevant geologic, hydrologic, and geochemical data.	Development of data bases from all available geologic, hydrologic, and geochemical data.
Parameter Uncertainties	Uncertainties in PTn parameters.	Conduct iterative calibration and validation studies to determine the effective parameters for process models, taking into account of all relevant data and observations.	Development of model parameter sets in agreement with all available geologic, hydrologic, and geochemical data.

Table 3.3.4-1. Average Percolation Fluxes (mm/yr) Simulated Within the Potential Repository Footprint for Thirteen Infiltration Scenarios

Infiltration Scenario	Average Surface Infiltration Rate[a]	Lower Bound			Mean			Upper Bound		
		Fracture	Matrix	Total	Fracture	Matrix	Total	Fracture	Matrix	Total
Interglacial[b]	--	0.20	0.06	0.26	4.02	0.52	4.54	11.59	0.26	11.85
Monsoon[b]	--	3.96	0.21	4.17	12.11	0.79	12.90	20.95	0.35	21.30
Intermediate[b]	--	1.59	0.15	1.74	19.51	0.94	20.45	38.50	0.49	38.99
OIS16 lower bound #1[c]	12.9	15.98	0.35	16.33	--	--	--	--	--	--
OIS16 lower bound #3[c]	36.0	27.72	0.44	28.16	--	--	--	--	--	--
OIS16 upper bound #1[c]	151.0	--	--	--	--	--	--	114.81	1.12	115.93
OIS16 mean #2[c]	87.9	--	--	--	70.57	1.74	72.31	--	--	--

Sources: [a] Preliminary work described in Bodvarsson 2001 [DIRS 154669], Attachment 12. Based on data associated with BSC 2001 [DIRS 154564].
[b] Lower bound, mean, and upper bound: CRWMS M&O 2000 [DIRS 122797], Section 6.6.
[c] Bodvarsson 2001 [DIRS 154669], Attachment 12.

Table 3.3.4-2. Summary of Uncertainty Issues Related to Three-Dimensional Flow Fields

Category	Uncertainty Issue	Treatment of Uncertainty Issue	Affected Goals
Conceptual Uncertainties	Effect of large gridblock averaging on flow field and grid resolution	Sensitivity analyses using different size gridblock models Examining modeling results against various types of observation data	Detailed distribution of percolation flux Smearing fronts in simulated tracer transport plumes or early breakthrough at water table
	Steady-state ambient moisture flow assumption	Sensitivity analyses with transient infiltration maps in PTn absent areas Investigate PTn dampening effects using modeling with pneumatic and isotopic data	Simulated percolation flux Estimated groundwater travel times in the UZ
	Ability of model to induce flow focusing	Stochastic modeling studies of fracture networks and permeability distributions Corroborated with seepage test data Alternative conceptual models for faults	Estimated fast flow pathways/weeps Input data to drift seepage models
	Model used to calculate fracture and matrix flow components and to handle fracture/matrix interactions	Sensitivity modeling studies using alternative dual-continuum conceptual models, such as MINC Use of hybrid model grids for different units, including discrete fracture and single porous media models	Estimated fracture/matrix flow components Radionuclide transport times in the UZ
	Layer-averaged rock properties	Proposed sensitivity analyses with laterally heterogeneous rock properties	Simulated flow focusing Input data to drift seepage models
	Transition of flow between porous-medium and fractured units	Corroborate with isotopic data and seepage tests in these areas, such as interface between PTn/TSw and CHv/CHz	Estimated fracture/matrix flow components in TSw and CHn
	Flow within/below perched water zones	Sensitivity analyses using different conceptualizations of CHn zeolitic fracture properties	Distribution of percolation flux below the repository horizon Estimated groundwater travel and radionuclide transport times in the UZ
	Applicability of van Genuchten's model to unsaturated fracture flow	Proposed tests with alternative moisture functions, such as Brook-Corey relations	Predicted moisture condition within fracture and matrix systems

Table 3.3.4-2. Summary of Uncertainty Issues Related to Three-Dimensional Flow Fields (Continued)

Category	Uncertainty Issue	Treatment of Uncertainty Issue	Affected Goals
Data Uncertainties	Uncertainties in upstream models (climate/infiltration, integrated site model)	Sensitivity and bounding modeling studies using various climate/infiltration scenarios Proposed sensitivity analyses using different geostatistical realizations of the distribution of mineral alteration with CHn	Predicted groundwater travel and radionuclide transport times in the UZ
	Uncertainties in data used to calibrate and validate UZ flow fields (e.g., fracture and fault parameters)	Proposed re-evaluation of air-permeability ≅ liquid permeability assumption for fractures Proposed sensitivity analyses and re-estimation of model parameters using refined grid resolution Proposed sensitivity analyses using heterogeneous distributions of key hydrologic parameters	Predicted moisture condition and percolation flux within fracture and matrix systems
Parameter Uncertainties	Uncertainties in UZ flow parameters, specifically fracture properties in CHn and fault properties	Reestimate fracture parameters using Busted Butte data Sensitivity studies with different fracture and fault properties	Predicted flow paths and groundwater travel times in the UZ
	Average percolation flux	Sensitivity modeling analyses with bounding-scenario infiltration rates	Groundwater water travel and tracer transport times in the UZ

Table 3.3.5-1. Summary of Numerical Model Cases for Mountain-Scale Thermal Hydrologic

Case No.	Numerical Grid	Thermal Load	Thermal Properties
1	3-D submodel, no drifts	67.7 kW/acre (1.35 kW/m); 80% forced ventilation for 300 years	Base 3-D case, no lithophysal cavities
2	3-D submodel, no drifts	67.7 kW/acre (1.35 kW/m); 80% forced ventilation for 300 years	3-D case, with lithophysal cavities
3	2-D cross section (NS#2) with locally defined drifts	67.7 kW/acre (1.35 kW/m); with 70% forced ventilation for 50 years	2-D, no lithophysal cavities
4	2-D cross section (NS#2) with locally defined drifts	67.7 kW/acre (1.35 kW/m); with 70% forced ventilation for 50 years	2-D, with lithophysal cavities
5	2-D cross section (NS#2) with locally defined drifts	67.7 kW/acre (1.35 kW/m); with 80% forced ventilation for 300 years	2-D, no lithophysal cavities
6	2-D cross section (NS#2) with locally defined drifts	67.7 kW/acre (1.35 kW/m); with 80% forced ventilation for 300 years	2-D, with lithophysal cavities
7	2-D cross section (NS#2) with locally defined drifts	67.7 kW/acre (1.35 kW/m); with 80% forced ventilation for 300 years	2-D, no lithophysal cavities, high infiltration, 5x mean

Source: Bodvarsson 2001 [DIRS 154669], Attachment 6.

NOTE: 2-D = two-dimensional; 3-D = three-dimensional.

Table 3.3.5-2. Recent Applications of TOUGH2 in Modeling Geothermal Systems

Site	Conditions, Phases	Physical Volume Modeled	Number of Model Elements	Calibration Method [a]	Length of Prediction Period	Calibration Inferences	Reference
Wairakei-Tauhara, New Zealand	2 phase	12 layers 3-D	1,417	NS, HM, P, T, w/ inverse modeling		More layers required	Bullivant and O'Sullivan 1998 [DIRS 144410]; O'Sullivan et al. 1998 [DIRS 154567]
Cerro Prieto, Mexico	1, 2 phase		347	NS, HM, P, T, many wells	2 Scenarios, 30 years	Location of upflow	Antunez et al. 1991 [DIRS 154568]
Nesjavellir, Iceland	2 phase	288 km^3 3-D	300	NS (100k years), HM (4 years)	30 years	Location of upflow zone	Bodvarsson et al. 1988 [DIRS 138603]; Bodvarsson et al. 1990 [DIRS 154574]; Bodvarsson et al. 1991 [DIRS 154575]; Bodvarsson et al. 1993 [DIRS 138618]
Kamojang, Indonesia	Vapor dominated	3-D	a) 456 b) 570	NS, P (20,000,000 years) HM, P (7 years)	30 years		O'Sullivan et al. 1990 [DIRS 137409]
East Olkaria, Kenya	2 phase	3 layers 3-D	150	HM, flow rate and enthalpy data (6.5 years)		High permeability region	Bodvarsson et al. 1987 [DIRS 136393]; Bodvarsson et al. 1987 [DIRS 136391]; Bodvarsson et al. 1990 [DIRS 136384]; Pham et al. 1996 [DIRS 154569]
		8 x 12 km, 3 layers 3-D	252		Many scenarios, 30 years		Bodvarsson et al. 1987 [DIRS 136393]; Bodvarsson et al. 1987 [DIRS 136391]; Bodvarsson et al. 1990 [DIRS 136384]
Krafla, Iceland	2 phase	100 blocks each 1 - $8x10^4$ m^3 1-D, 2-D, 3-D	100	Well test data, NS, T, P (20,000 years), HM	8 - 30 years with caution		Bodvarsson et al. 1984 [DIRS 144397]; Bodvarsson et al. 1984 [DIRS 137136]; Bodvarsson et al. 1984 [DIRS 137139]
Krafla-Hvitholar, Iceland	1, 2 Phase	2-D	85	NS, 3 Wells, T, P	3 Scenarios, 10 years	Importance of fault	Tulinius and Sigurdsson 1989 [DIRS 154571]
Amatitlan, Guatemala	2 Phase	140 km^3, 5 layers 3-D	1,220	NS T, P, HM (well flow testing ~30 days)	30 years with caution		Pham et al. 1996 [DIRS 154569]
Zunil, Guatemala	Vapor dominated	16 km^3 3-D	459	NS, T, P, well test data, interference test		Secondary upflow zone	Menzies et al. 1991 [DIRS 137923]

NOTE: [a] NS = Natural State; HM = History Matching; T = Temperature; P = Pressure; 2-D = two-dimensional; 3-D = three-dimensional.

Table 3.3.5-3. Summary of Uncertainty Issues Related to Thermal Hydrologic Effects on Mountain-Scale Flow

Category	Uncertainty Issue	Treatment of Uncertainty Issue	Affected Goals
Conceptual Uncertainties	Ventilation effect and heat transfer mechanism: Heat is evenly distributed within the drifts and all the waste is emplaced at time zero Ventilation removes only heat and not vapor Top and bottom boundaries are represented by fixed temperature, pressure, and saturation boundary Perched water does not affect TH processes at repository	Effects of thermal load variability not important beyond 100 years. All waste emplaced at time zero is a conservative approach When drift walls are dry then ventilation removes primarily heat Boundaries are far from repository Most Perched water up to 150 m below repository (CRWMS M&O 2000 [DIRS 144454], Section 5)	Maximum temperature Predicted liquid and gas flux UZ PTn, CHn, and water table temperature. Surface temperature (top of model) When close to drift impact on liquid flux and temperature
Data Uncertainties	Uncertainties in data used to calibrate and validate mountain-scale TH model	Data used in TH model are best available for mean UZ thermal and flow properties (CRWMS M&O 2000 [DIRS 144454], Section 4) Addressed by stochastic model used in Section 4.3.5	All
Parameter Uncertainties	Uncertainties in mountain-scale thermal properties: Drifts are assigned matrix and fractures properties of hydrogeological units in which they are located Thermal and flow properties not affected by temperature. Assumption supported by THM and THC analysis No hysteresis in flow properties	Effects of excavation and backfill are not important for the time scale considered (Section 4.3.4) Effects of TM-THC coupling are not significant especially in the lower temperature operating mode (Sections 3.3.6, 4.3.6, 4.3.7) Hysteresis effects are small (CRWMS M&O 2000 [DIRS 144454], Section 5)	Liquid flux and temperature (<100 yrs after emplacement) TM- and THC-process effects only long-term seepage

Table 3.3.6-1. Minerals, Aqueous Species, and Gaseous Species in the Mountain-Scale Thermal-Hydrologic-Chemical Model

Aqueous Species (primary)	Gaseous Species (primary)	Minerals
H_2O	CO_2	Calcite
H^+	H_2O	Tridymite
Na^+	Air	α–Cristobalite
K^+		Quartz
Ca^{+2}		Amorphous Silica
Mg^{+2}		Hematite
SiO_2		Fluorite
AlO_2^-		Gypsum
$HFeO_2^{-2}$		Goethite
HCO_3^-		Albite
Cl^-		K-Feldspar
SO_4^{-2}		Anorthite
F^-		Ca-Smectite
		Mg-Smectite
		Na-Smectite
		Opal
		Illite
		Kaolinite
		Glass
		Stellerite
		Heulandite
		Mordenite
		Clinoptilolite

Source: BSC 2001 [DIRS 154677], Table 8.

Table 3.3.6-2. Summary of Uncertainty Issues Related to the Prediction of Thermal Hydrologic-Chemical Effects on Mountain-Scale Unsaturated Zone Flow and Geochemistry

Category	Uncertainty Issue	Treatment of Uncertainty Issue	Affected Goals
Conceptual uncertainties	Effect of 3-D TH processes on mountain-scale geochemistry	Treated indirectly by evaluation of 2-D TH processes on geochemistry (this work)	Limits range of possible water compositions and amounts of mineral alteration owing to focused gas and liquid flow
	Impact of heating SZ on gas chemistry in UZ	Not treated	CO_2 degassing of SZ water could affect post-thermal water chemistry
	Surface temperature assumed constant instead of variable	Not treated	Variable surface temperature could result in more near-surface focusing of heat and vapor, and enhanced percolation flux around these areas
	Changes in infiltrating water chemistry associated with climate changes	Assessed indirectly through drift-scale-THC simulations using alternate water compositions	Results in more uncertainty of range in potential chemical compositions during post-thermal period
	Uncertainty in flow below potential repository and conceptual models for perched water	Not treated	Reaction rates in CHn zeolitic and vitric units are related to fluid fluxes as well as heat and therefore the different conceptual models for perched water may lead to a larger range in uncertainty for mineral alteration and effects on flow and transport
	Uncertainty in spatial distribution of net infiltration	Treated indirectly in drift-scale THC models through evaluation of different infiltration rates Larger-scale effects of different spatial distributions on flow focusing and THC processes not treated	Limits range of possible water compositions and distribution of mineral precipitation and dissolution
Data uncertainties	Uncertainties in mineralogy in repository unit	Treated indirectly by evaluation of mineralogy from two different geologic columns in drift-scale THC models Little data from Calico Hills unit under the potential repository footprint to constrain mineralogical abundances and variability	Limits prediction of potential effects on flow and transport in the Calico Hills unit, where glass, zeolite, and clay abundances are highly variable
	Thermodynamic and kinetic data specifically for zeolites, clays and glass	Treated through sensitivity studies on long-term behavior of ambient system water and gas chemistry and mineralogy assuming a fixed infiltration rate (BSC 2001 [DIRS 154677]) Many uncertainties unknown and should be treated through laboratory experiments under thermal conditions relevant to alteration of Calico Hills unit	Adds uncertainty to ranges of predicted water compositions, mineral assemblages, and changes in hydrologic properties

Table 3.3.6-2. Summary of Uncertainty Issues Related to the Prediction of Thermal Hydrologic-Chemical Effects on Mountain-Scale Unsaturated Zone Flow and Geochemistry (Continued)

Category	Uncertainty Issue	Treatment of Uncertainty Issue	Affected Goals
Parameter uncertainties	Uncertainties in fault parameters	Not treated	Faults may amplify THC processes because of their role as potential conduits for vapor and liquid flow and as a capillary barrier and therefore the range of potential effects have more uncertainty
	Large scale heterogeneity	Large-scale heterogeneity in mineralogical properties treated in part through variation in zeolitic or vitric attributes for layers and their changes in thickness	Heterogeneity in mineralogical properties could amplify local effects on hydrologic properties
	Uncertainty propagation	Treated preliminarily through alternate mineral reaction rates	Limits assessment of THC effects on flow, transport, and geochemistry in the UZ, and of uncertainty for TSPA

Table 3.3.7-1. Thermal-Hydrologic-Mechanical Parameter Data Used in Current Simulation

Parameter	Tptpmn	Tptpll	Source
Young's modulus	14.77 GPa	14.77 GPa	Extracted directly from CRWMS M&O 1999 [DIRS 126475], Table 10 to 15, and Table 24.
Poisson's ratio	0.21	0.21	
Thermal expansion coefficient	4.14 E-6 /°C	4.14 E-6 /°C	
Tensile strength	1.54 MPa	1.54 MPa	
Initial hydraulic aperture for Equation (4.3.7-2), b_i	286.9 µm	440.8 µm	The value of b_i is calculated from mean fracture spacing, *s*, and isotropic permeability, *k*, (CRWMS M&O 2000 [DIRS 144426], Section 6.1.4), assuming an ideal cubic block model, leading to the following formula: $b_i = \sqrt[3]{k \times 6 \times s}$.
Maximum joint closure for Equation (4.3.7-2), b_{max}	1486.0 µm	1486.0 µm	Model calibration against air-permeability experiments at Niches and DST (see Section 4.3.7.4.3), adjusted to a case of larger initial aperture. b_{max} is increased for the mountain scale properties compared to the calibrated value for the drift scale properties (Table 4.3.7-4) to match the maximum permeability increase observed at a initial permeability range of 1.7 to 4.5 $\times 10^{-11}$ m^2 (Figure 4.3.7-7), and to limit the possible permeability reduction less than 0.1 as observed in the DST.
Exponent for Equation (4.3.7-2), α	1.1 E-6	1.1 E-6	
Vertical stress gradient, σ_v	0.022 MPa/m	0.022 MPa/m	Within range of field measurements by Stock et al. 1985 [DIRS 101027] and Lee and Haimson 1999 [DIRS 129667].
Horizontal stress, σ_h	0.35 $\times$ σ_v MPa	0.35 $\times$ σ_v MPa	

Table 3.3.7-2. Changes In Permeability for Hydrostratigraphic Layers at the Mid-Repository Symmetry Boundary on the Left Side of the Model

Units	Elevation (m)	K_v/K_i	K_H/K_i
TCw	1447–1326	1.0 to 38	1.0 to 38
PTn	1326–1291	1.24 to 2.55	1.28 to 2.75
TSw31	1291–1289	1.80	2.27
TSw32	1289–1250	0.58	0.98
TSw33	1250–1167	0.40	0.72
TSw34 (Tptpmn)	1167–1134	0.28	0.66
TSw35 (Tptpll)	1134–1030	0.47 to 0.77	0.75 to 0.89
TSw36–37	1030–981	0.83 to 0.85	0.92 to 0.93
TSw38–39	981–960	0.53 to 0.72	0.80 to 0.88
CHn-pp4	960–869	0.9 to 1.0	1.0 to 1.1
Pp3_bf3	869–730	1.1 to 1.2	1.1 to 1.2

Source: Derived from Bodvarsson 2001 [DIRS 154669], Attachment 9, pp. 1 to 78.

NOTE: K_v = vertical permeability; K_H = horizontal permeability; K_i = initial permeability.

Table 3.3.7-3. Summary of Uncertainty Issues Related to Thermal-Hydrologic-Mechanical Effects on Mountain-Scale Flow

Category	Uncertainty Issue	Treatment of Uncertainty Issue	Affected Goals
Conceptual Model Uncertainties	Effects of THM processes versus TH only.	Implement a coupled THM code, joining TOUGH2 V1.5 and FLAC3D V2.0 codes, to study the impact of THM processes (Section 3.3.7.3).	Flux above and around the potential repository.
	3-D versus 2-D flow patterns.	2-D calculations have been done (Section 3.3.7.4); 3-D calculations to be conducted.	Flux above and around the potential repository.
Model Geometry Uncertainties	Horizontally uniform layers versus realistic inclined layers.	Calculation with layers assumed to be horizontal have been done (Section 3.3.7.4). Realistic-geometry simulations could reduce uncertainty.	Flux above and around the potential repository.
	Boundary conditions used.	Sensitivity study with range of conditions could reduce uncertainty.	Flux above and around the potential repository.
	Layering structure at the potential repository site.	The vertical stratigraphy at one location has been simulated (Section 3.3.7.4). Variation of layering structure to be considered.	Flux above and around the potential repository.
Parameter Uncertainties	Rock fracture stiffness in the layers. Residue permeability values.	A simulation with conservative values of fracture stiffness and residual aperture have been done (Section 3.3.7.4). A complete THM analysis of the Drift Scale Heater test with supplementary measurements could reduce uncertainty.	Flux above and around the potential repository.
	Heterogeneity in permeability spatial distribution.	Additional simulations needed on heterogeneous field representing the hydrogeologic units. Studies with multiple realizations to be conducted.	Flux above and around the potential repository.
	Property parameter values.	Hydraulic and thermal property parameters to be confirmed for the different layers.	Flux above and around the potential repository.

INTENTIONALLY LEFT BLANK

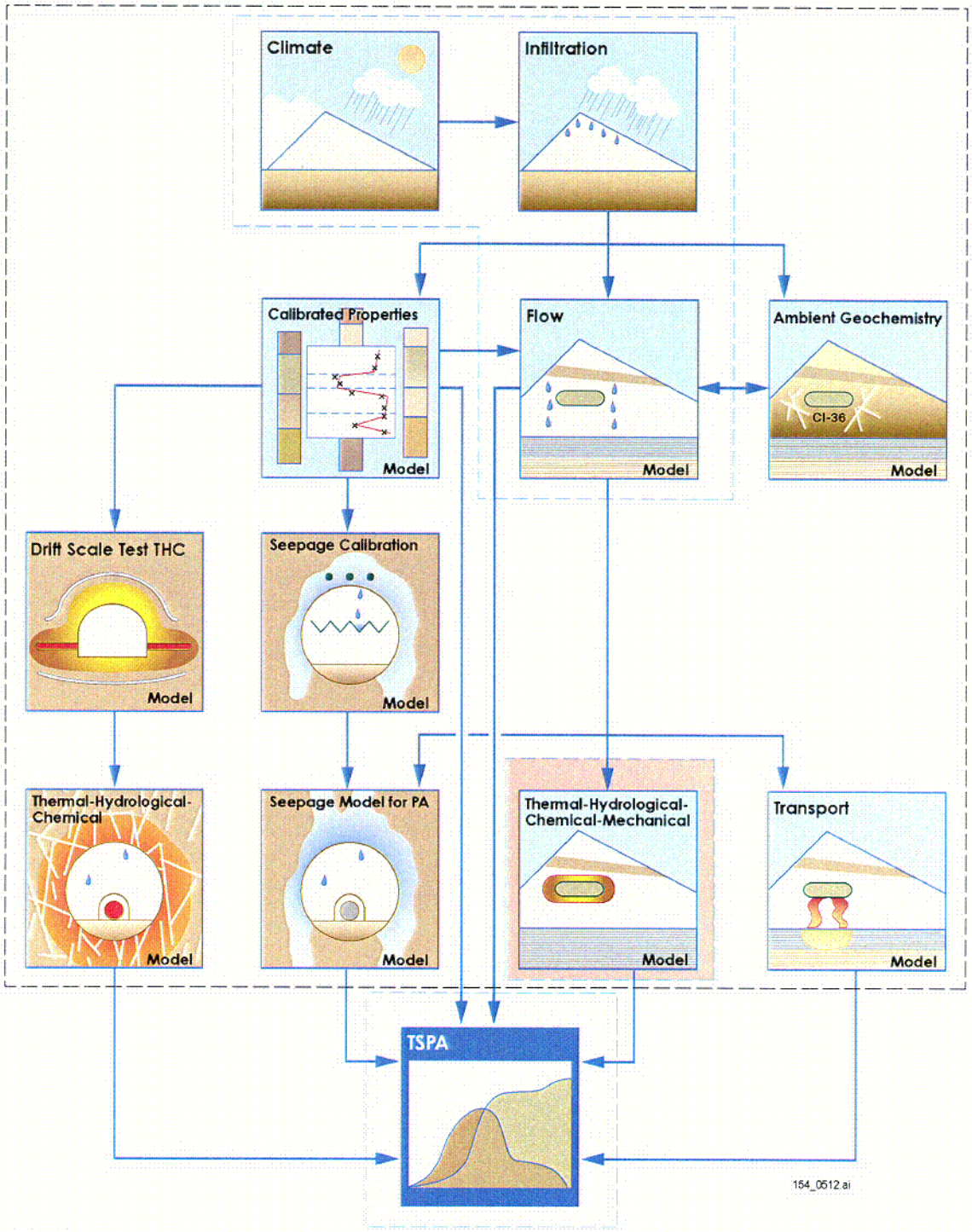

154_0512.ai

Source: Modified from CRWMS M&O 2000 [DIRS 151940], Figure 1-2.

NOTE: Most models relevant to this section are highlighted with color backgrounds.

Figure 3.1-1. Main Models Included in the Unsaturated Zone Process Model Report, Interrelations among them, and Connections to Total System Performance Assessment

C01

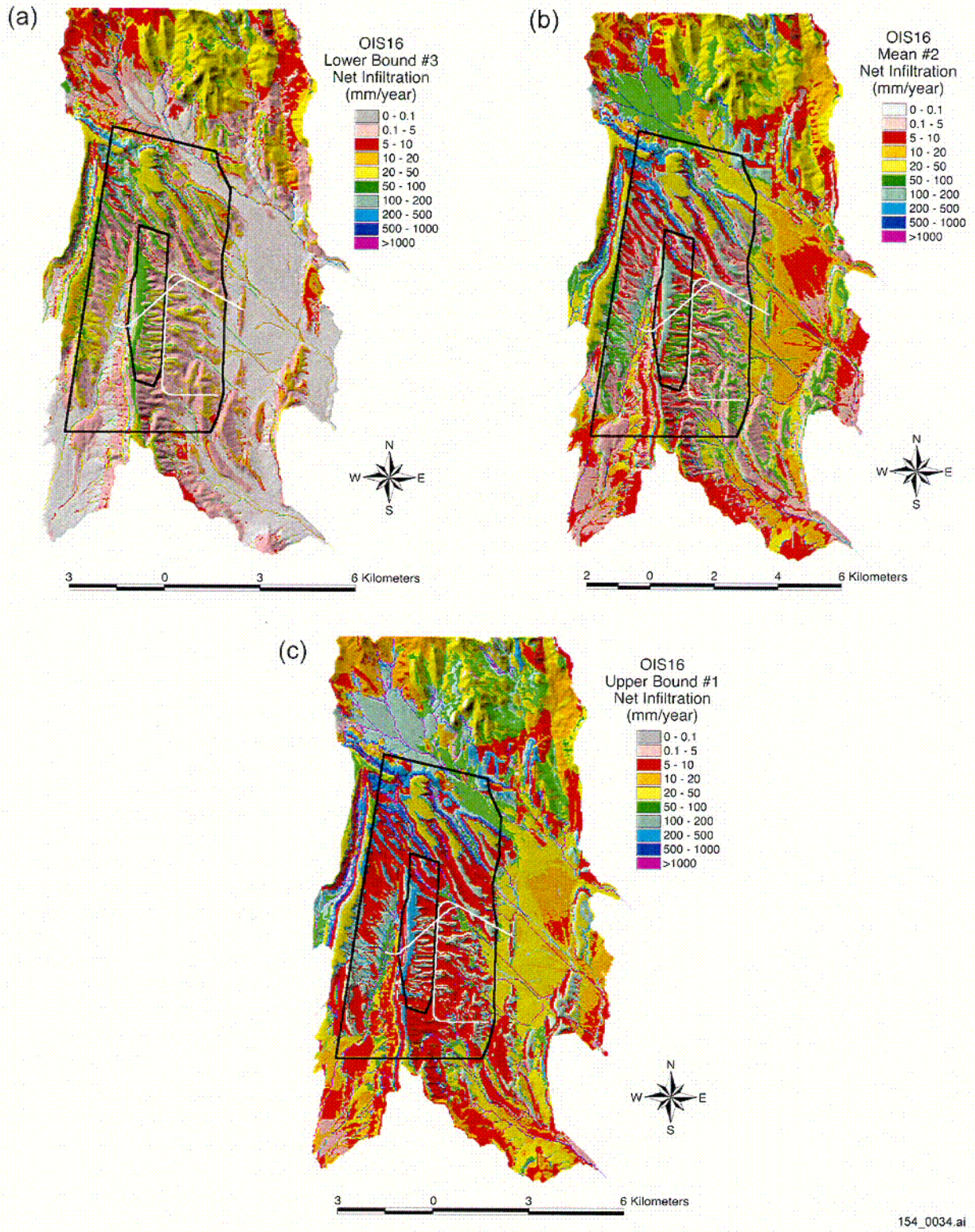

154_0034.ai
Source: BSC 2001 [DIRS 154873].

NOTE: Infiltration for lower (a), mean (b), and upper (c) bounds.

Figure 3.3.2-1. Net Infiltration for the Glacial Stage 6/16-Climate Scenario

C02

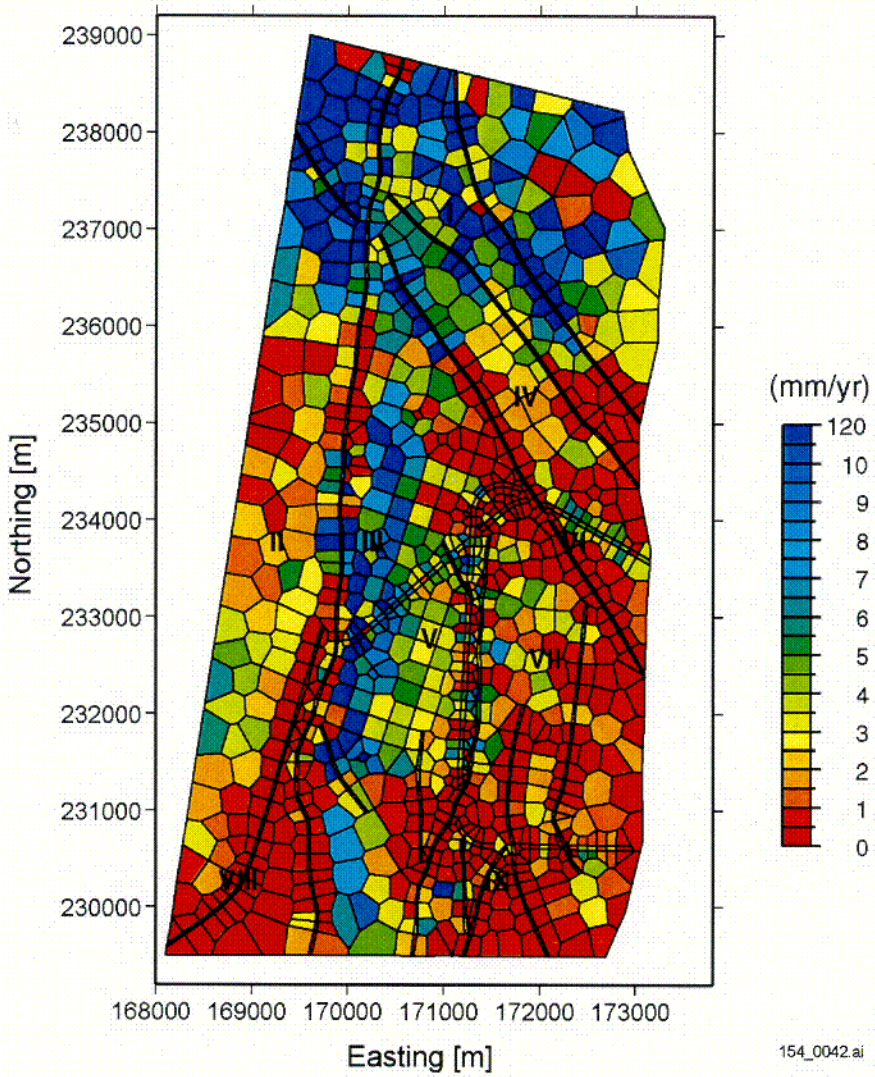

154_0042.ai

Source: DTN: GS000399991221.002 [DIRS 147022].

NOTE: Nevada coordinates in meters.

Figure 3.3.3-1. Present-Day Mean Net Infiltration

C03

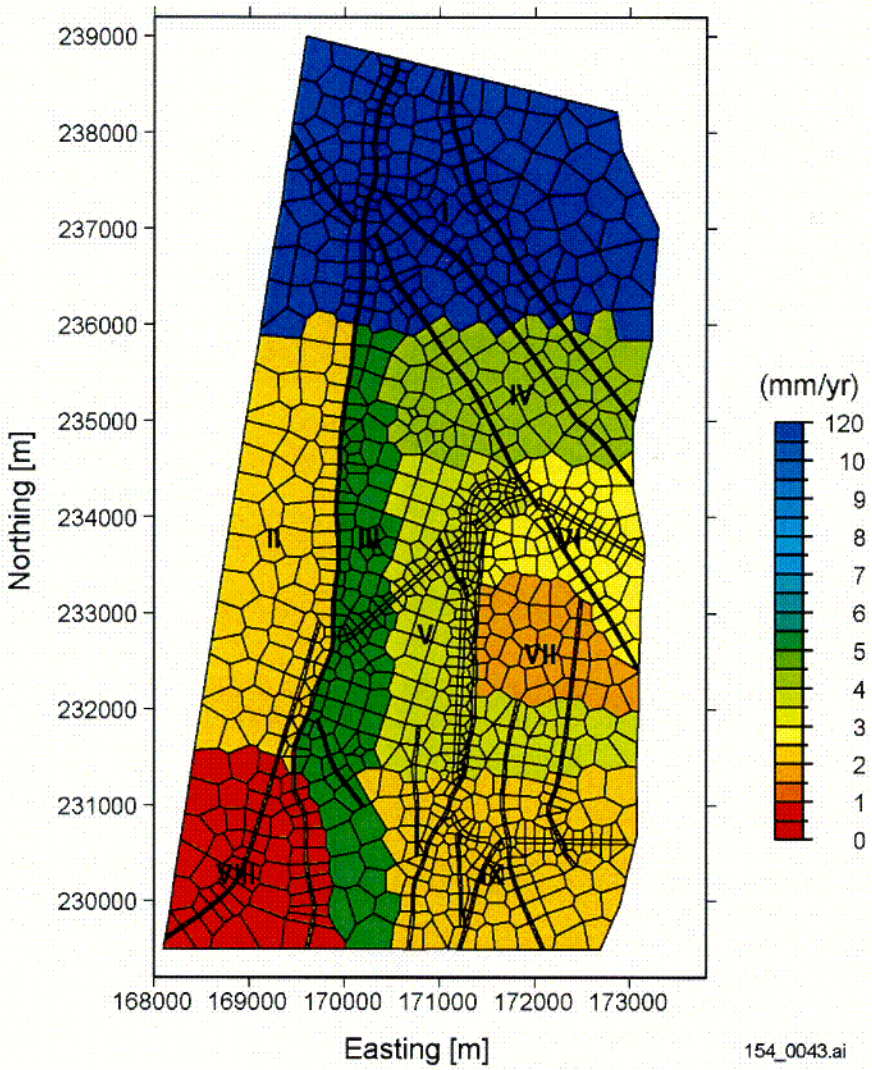

154_0043.ai

Source: Bodvarsson 2001 [DIRS 154669], Attachment 11, listed on p. 80.

NOTE: Uniform net infiltration in each region. Nevada coordinates in meters.

Figure 3.3.3-2. Chloride-Based, Present-Day Mean Net Infiltration

C04

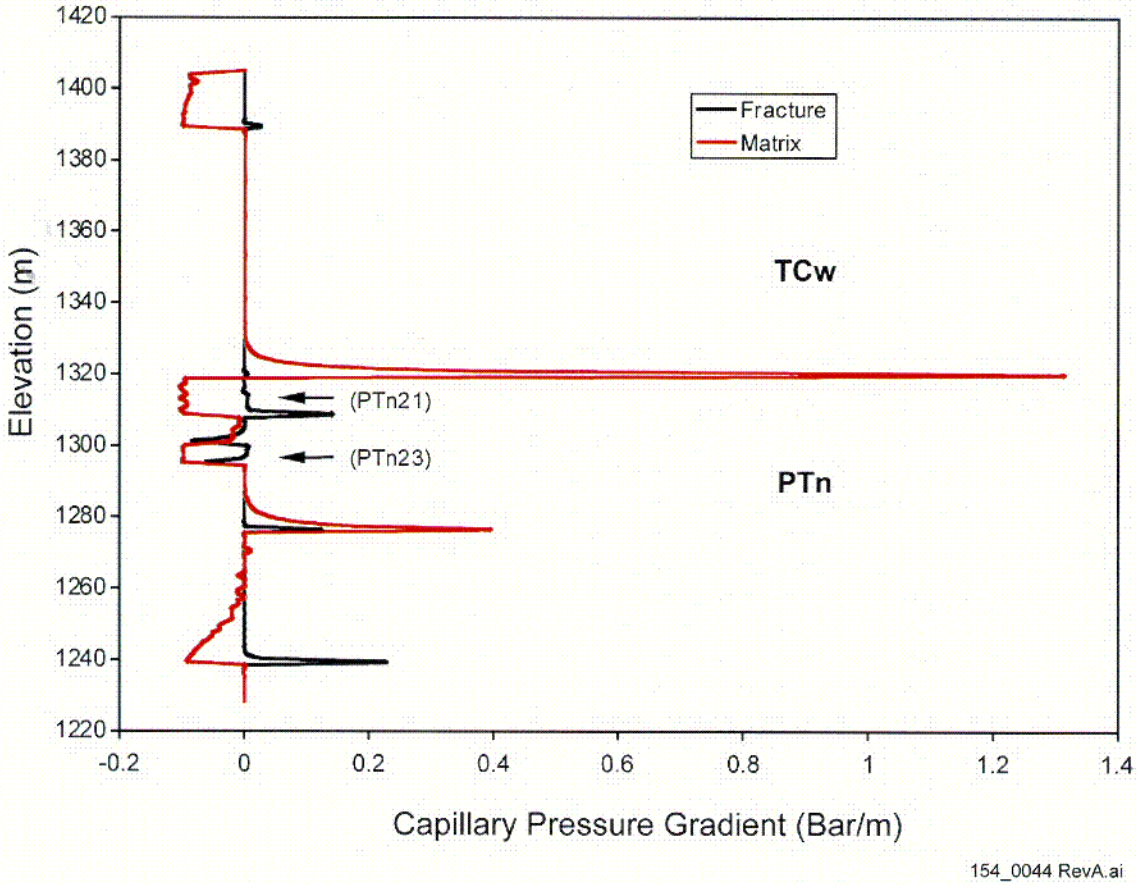

154_0044 RevA.ai

Source: Wu et al. 2001 [DIRS 154918], Figure 4.1-5.

NOTE: Capillary pressure measured in bar/m at coordinates 171200E, 235119N (coordinates using refined grid).

Figure 3.3.3-3. Vertical Capillary Pressure Gradients

C05

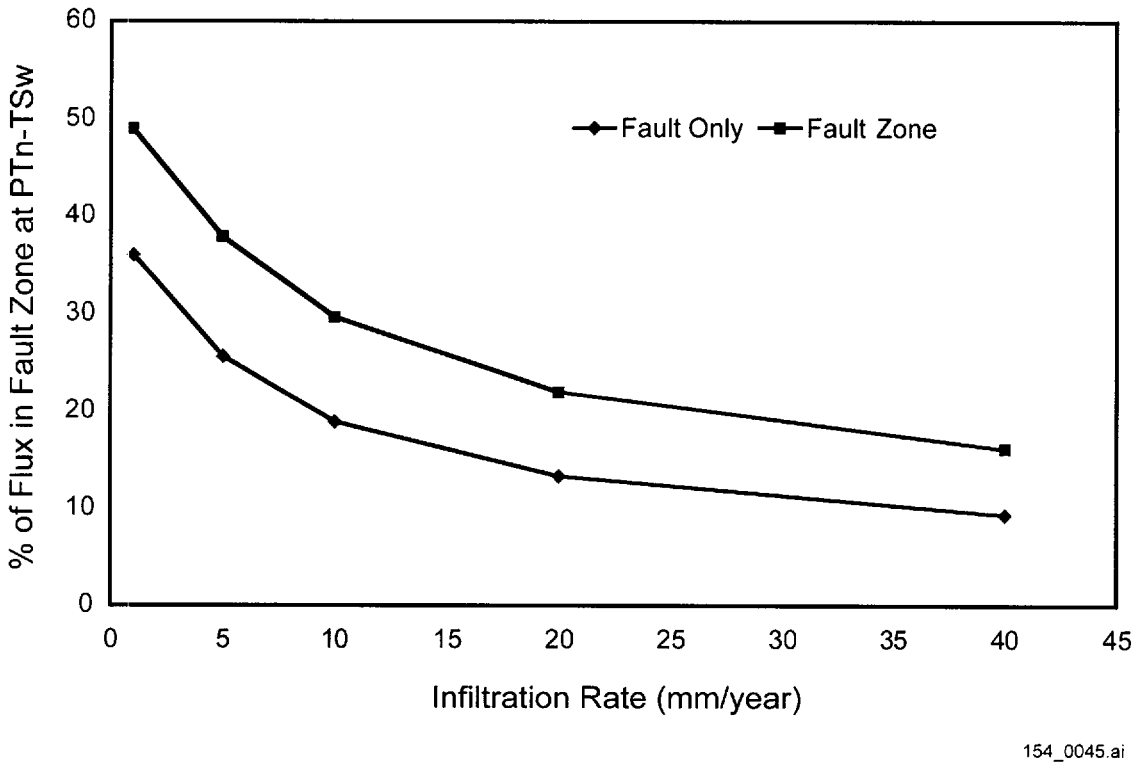

154_0045.ai

Source: Wu et al. 2001 [DIRS 154918].

NOTE: Effects of net infiltration values on percentage of flow through faults and fault zones, reflecting the amount of lateral water flow within the PTn unit along a vertical cross section, using the refined grid and uniform surface net infiltration pattern.

Figure 3.3.3-4. Effect of Net Infiltration on Percentage of Flow-Through Faults and Fault Zones

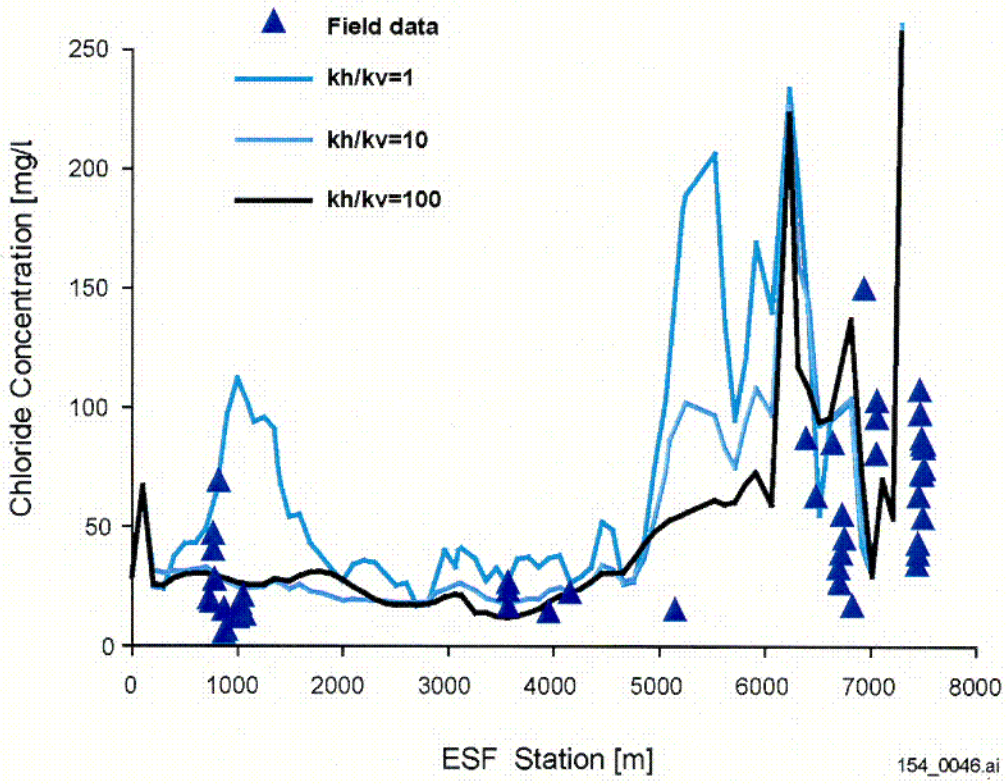

154_0046.ai

Source: Bodvarsson 2001 [DIRS 154669], Attachment 11, listed on p. 79.

NOTE: ESF = Exploratory Studies Facility; kh = horizontal permeability; kv = vertical permeability.

Figure 3.3.3-5. Effect of Horizontal Permeability on the Modeled Concentrations of Chloride in the Exploratory Studies Facility

C06

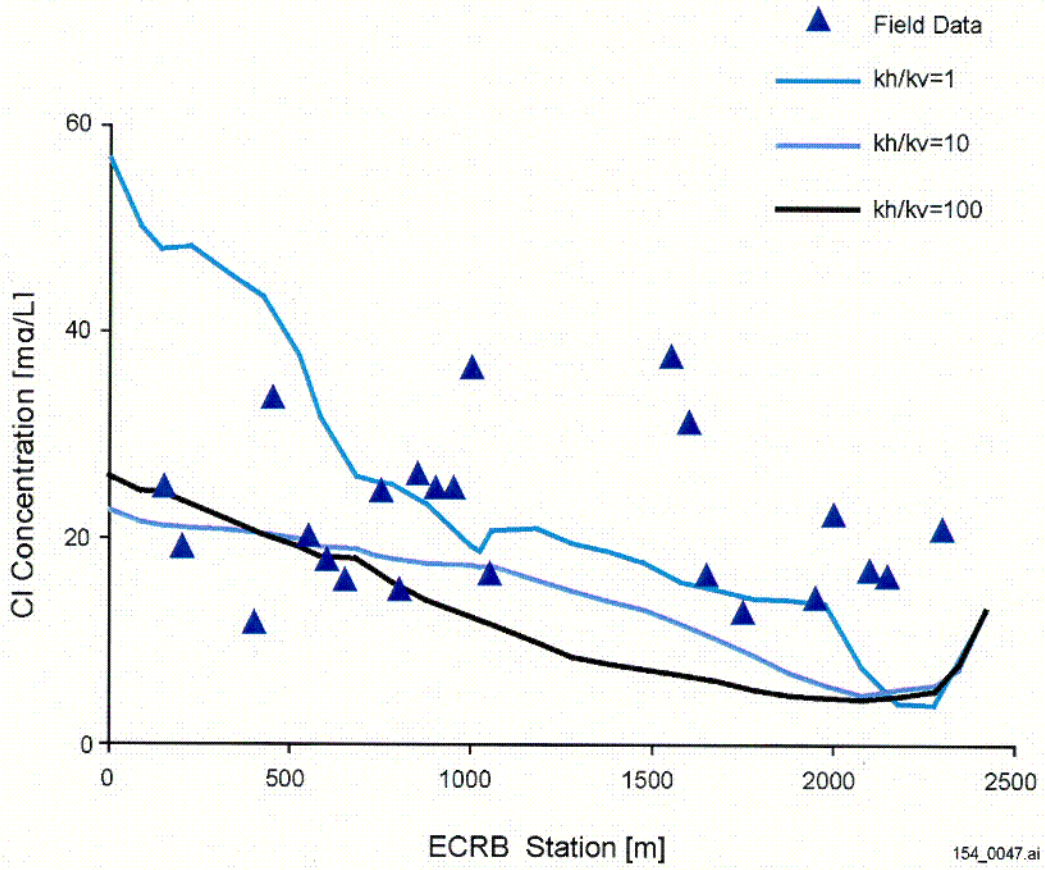

154_0047.ai

Source: Bodvarsson 2001 [DIRS 154669], Attachment 11, listed on p. 79.

NOTE: Model assumes infiltration at present-day mean rates. Cl = chloride; ECRB = Enhanced Characterization Repository Block.

Figure 3.3.3-6. Effect of Horizontal Permeability on the Modeled Concentrations of Chloride in the Enhanced Characterization Repository Block

C07

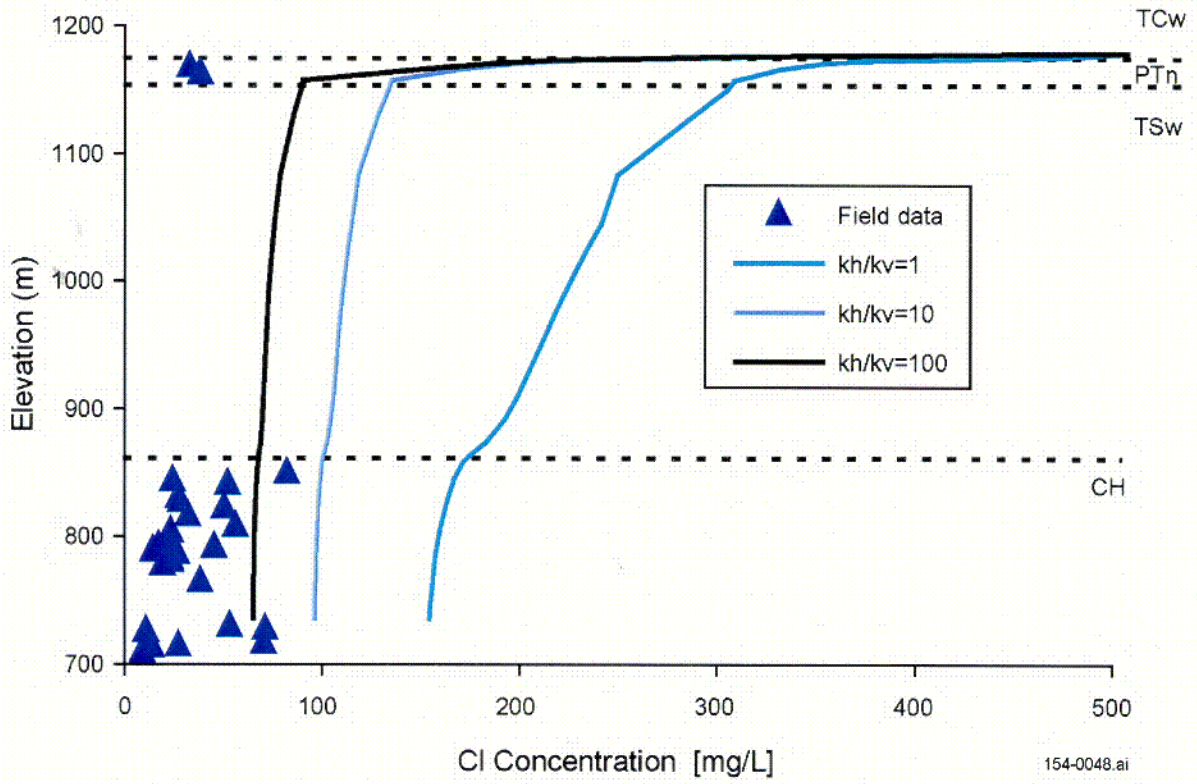

154_0048.ai

Source: Bodvarsson 2001 [DIRS 154669], Attachment 11, listed on p. 79.

Figure 3.3.3-7. Effect of Horizontal Permeability on the Modeled Concentrations of Chloride in Borehole UZ#16.

C08

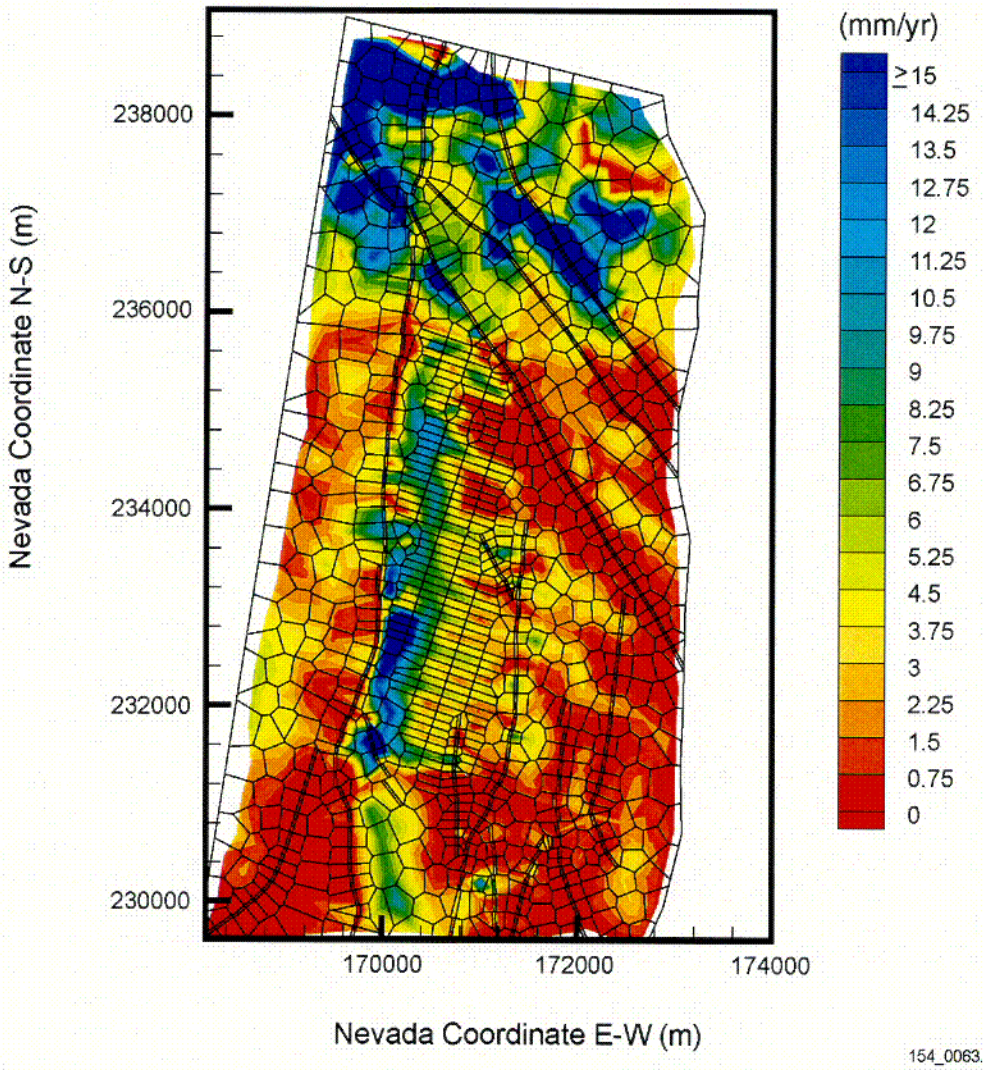

154_0063.ai

Sources: CRWMS M&O 2000 [DIRS 122797], Figure 6-3; DTN: GS000399991221.002 [DIRS 147022]; DTN: LB990801233129.003 [DIRS 122757].

NOTE: Simulation uses present-day, base-case, mean infiltration.

Figure 3.3.4-1. Plan View of Total System Performance Assessment Grid and Net Infiltration Distributed Over the Domain of the Unsaturated Zone Model

C09

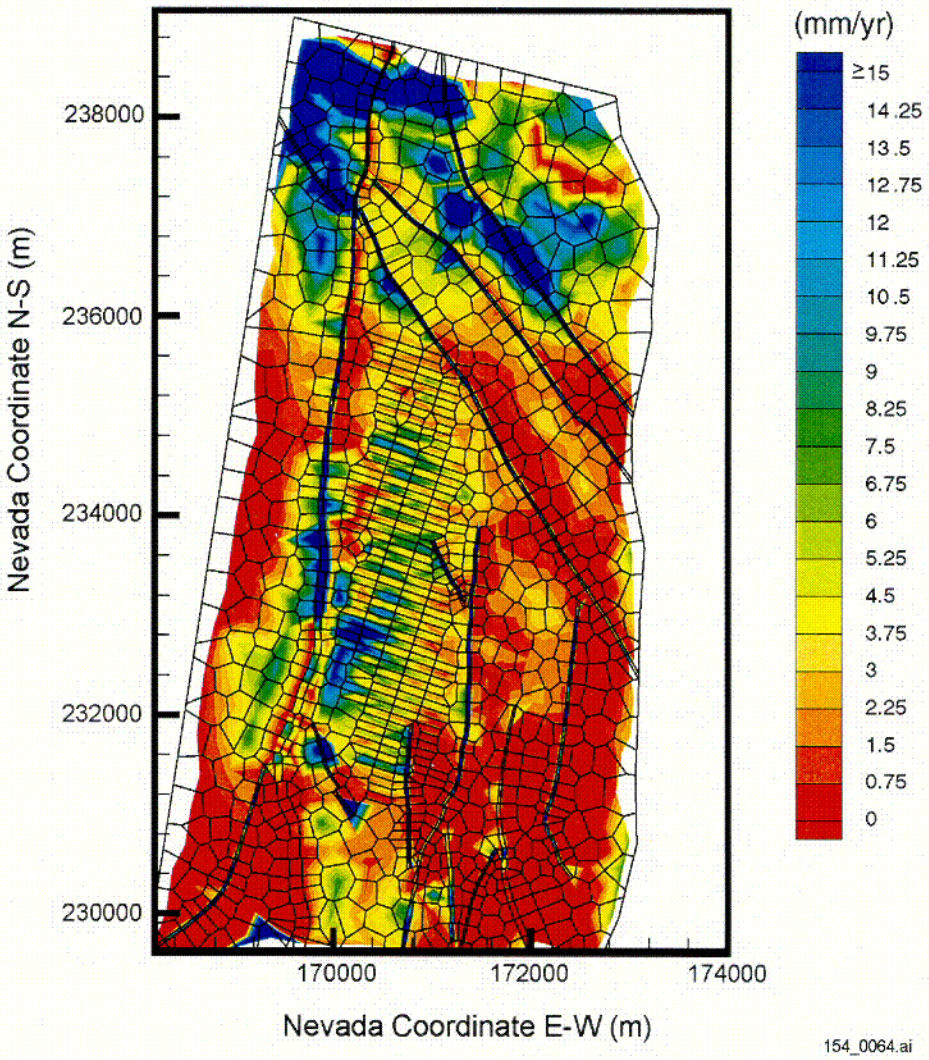

154_0064.ai

Source: CRWMS M&O 2000 [DIRS 122797], Figure 6-42.

NOTE: Simulation uses present-day, mean infiltration.

Figure 3.3.4-2. Simulated Percolation Flux at the Repository Horizon for the Flow-Through Perched Water Conceptual Model

C10

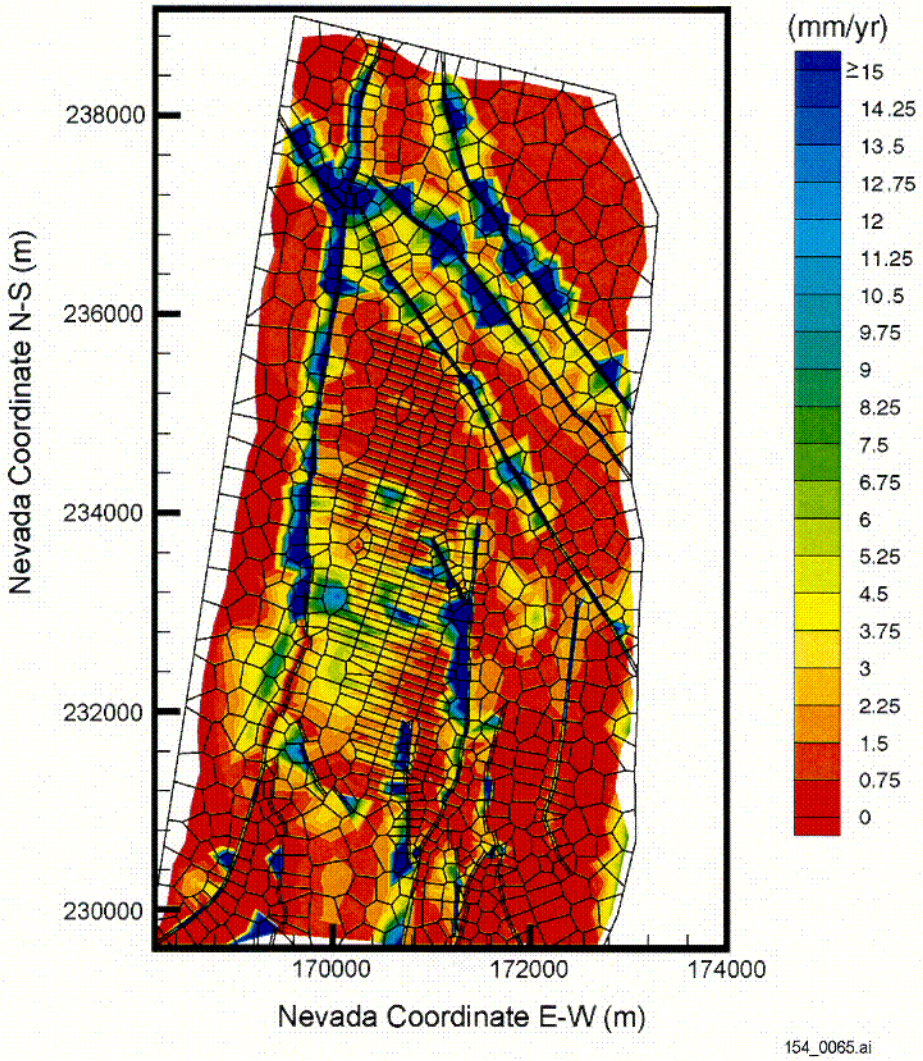

154_0065.ai

Source: CRWMS M&O 2000 [DIRS 122797], Figure 6-45; DTN: LB990801233129.003 [DIRS 122757].

NOTE: Simulation uses present-day, mean infiltration.

Figure 3.3.4-3. Simulated Percolation Flux at the Water Table for the Flow-Through Perched Water Conceptual Model

C11

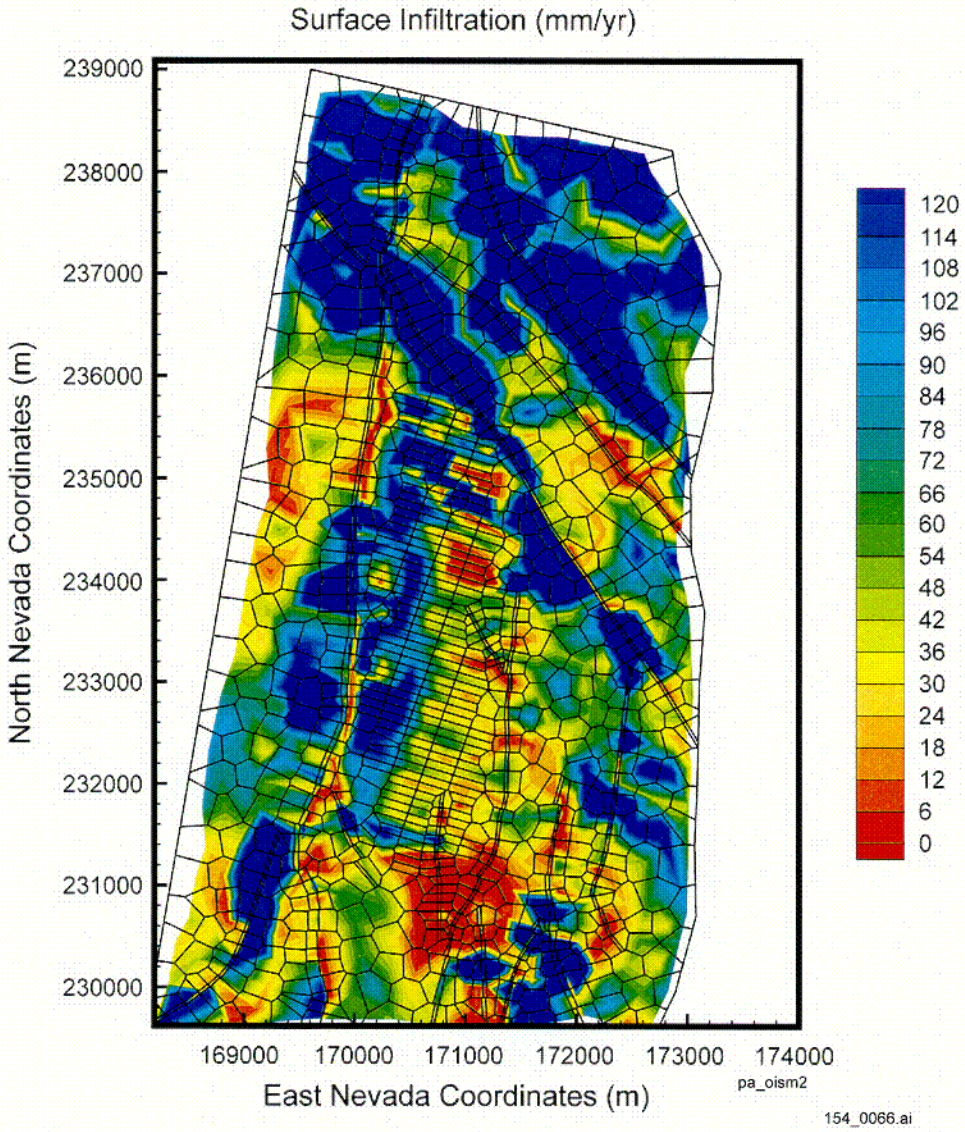

154_0066.ai

Source: Preliminary work described by Bodvarsson 2001 [DIRS 154669], Attachment 12, pp. 208 to 209; also based on data associated with BSC 2001 [DIRS 154564].

NOTE: Model assumes the full-glacial, mean #2 infiltration scenario.

Figure 3.3.4-4. Plan View of Net Infiltration Distributed Over the Domain of the Three-Dimensional Unsaturated Zone Total System Performance Assessment Model

C12

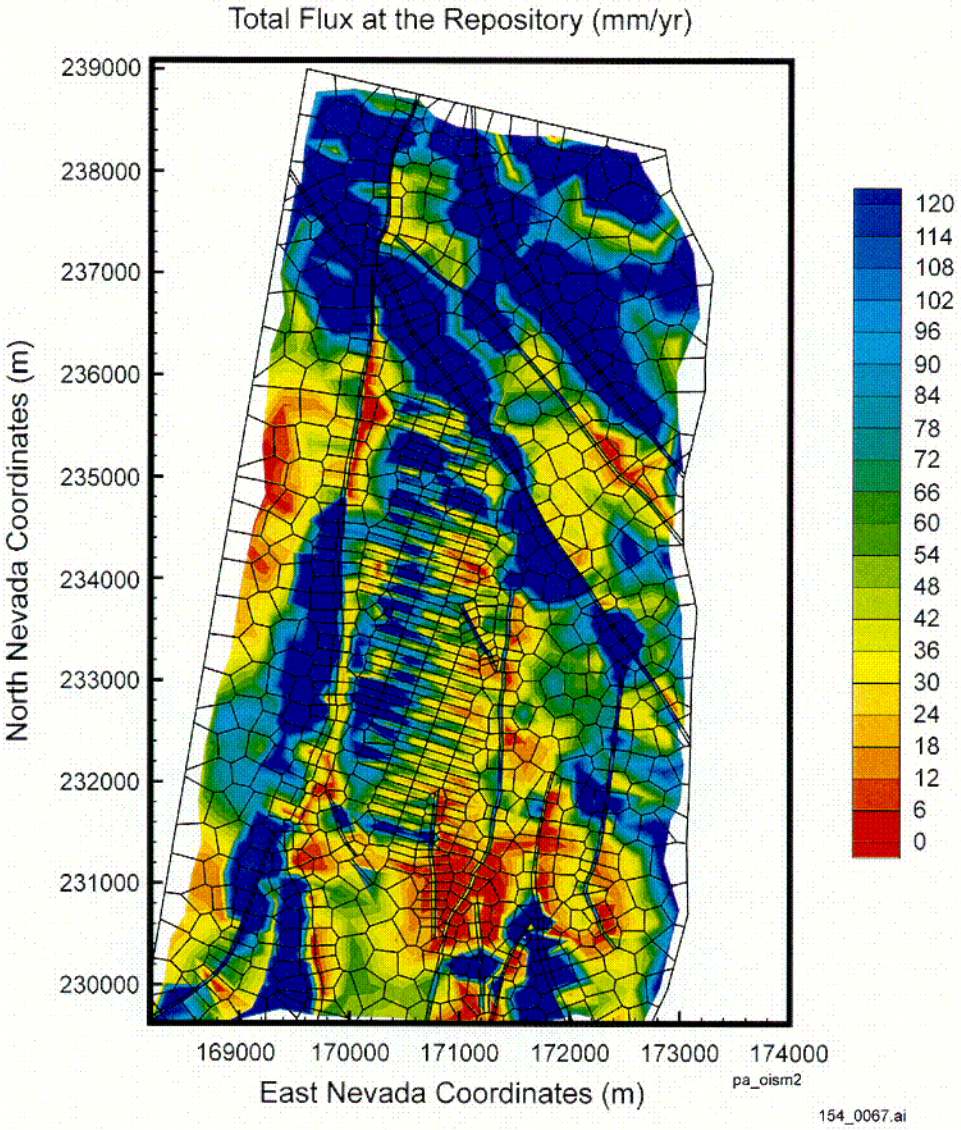

154_0067.ai

Source: Preliminary work described by Bodvarsson 2001 [DIRS 154669], Attachment 12, file listed on p. 209.

NOTE: Simulation uses the flow-through perched water conceptual model.

Figure 3.3.4-5. Simulated Percolation Flux at the Potential Repository Horizon under the Full-Glacial, Mean #2 Infiltration Scenario

C13

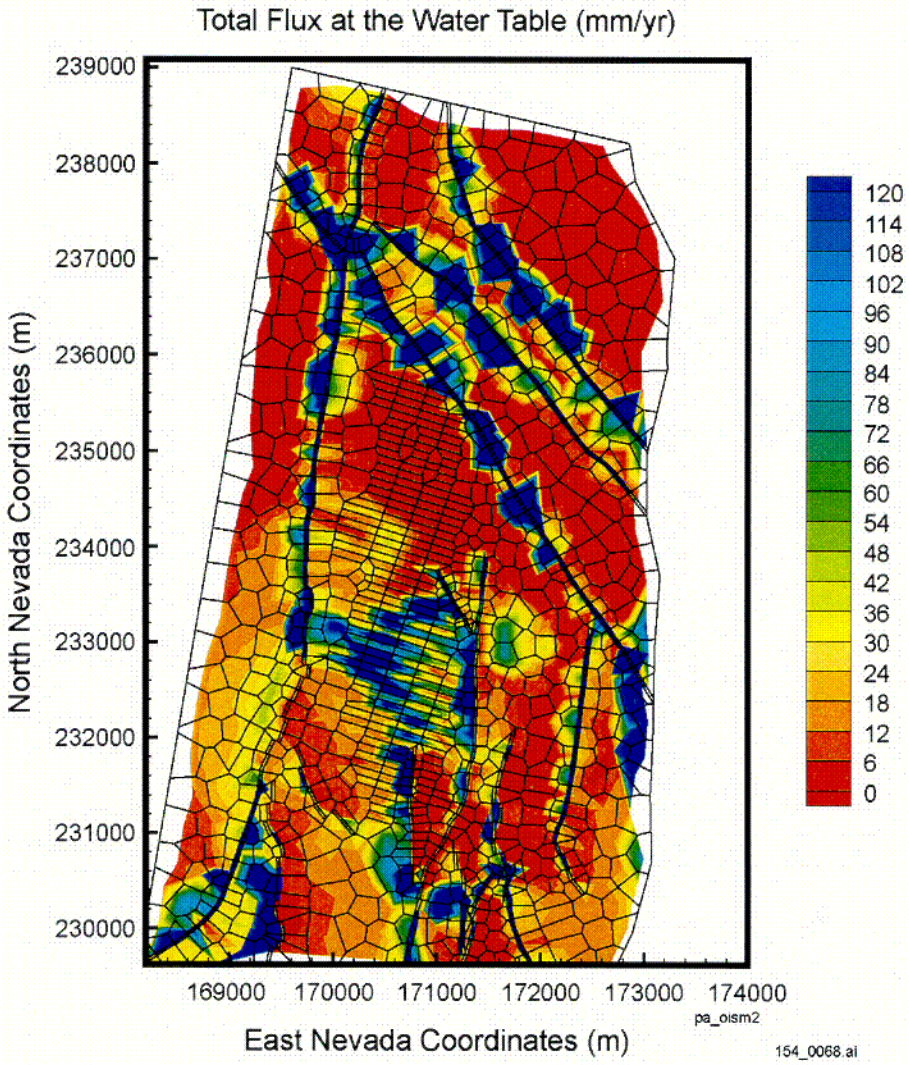

154_0068.ai

Source: Preliminary work described by Bodvarsson 2001 [DIRS 154669], Attachment 12, file listed on p. 209.

NOTE: Simulation uses the Flow-Through Perched Water Conceptual Model.

Figure 3.3.4-6. Simulated Percolation Flux at the Water Table under the Full-Glacial, Mean #2 Infiltration Scenario

C14

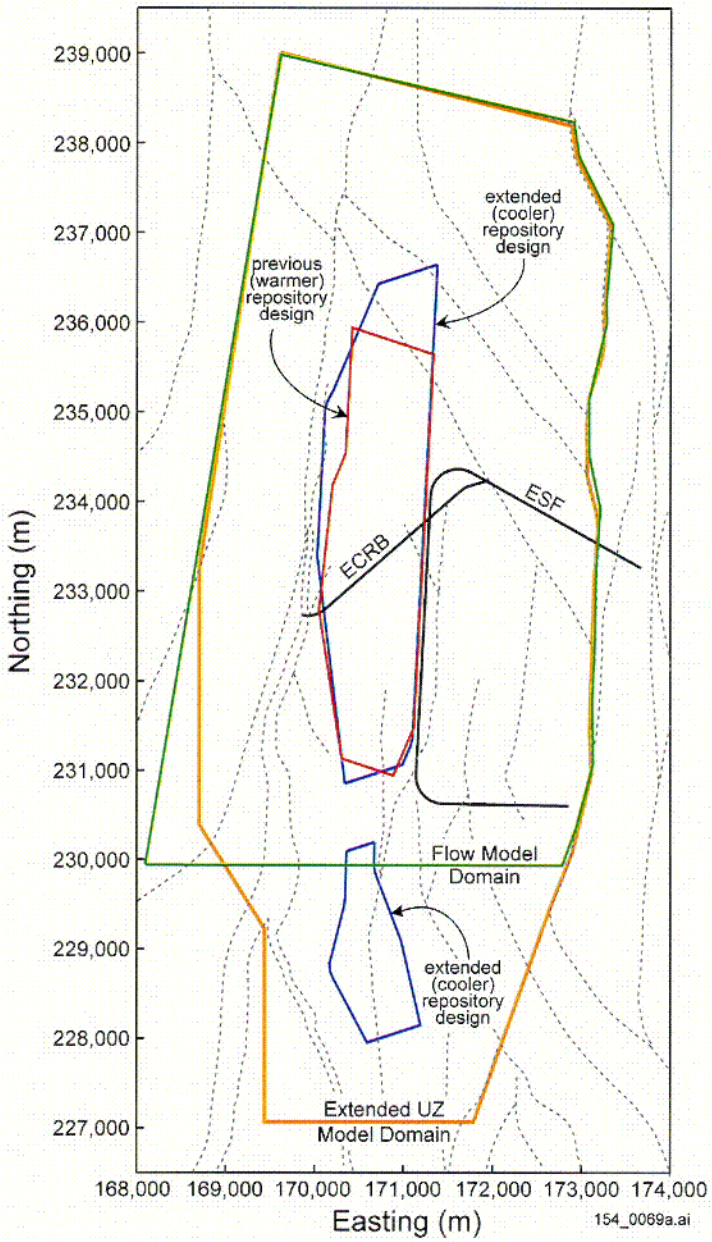

154_0069a.ai

Sources: DTN: MO9901MWDGFM31.000 [DIRS 103769]. References for repository layouts: Extended BSC 2001 [DIRS 154548]; Previous CRWMS M&O 1997 [DIRS 100245].

NOTE: Dotted lines represent faults as mapped in the Geologic Framework Model version 3.1. Nevada coordinates in meters. ECRB = Enhanced Characterization of the Repository Block; ESF = Exploratory Studies Facility; UZ = unsaturated zone.

Figure 3.3.4-7. Plan View of Unsaturated Zone Model Domains and Potential Repository Layouts

C15

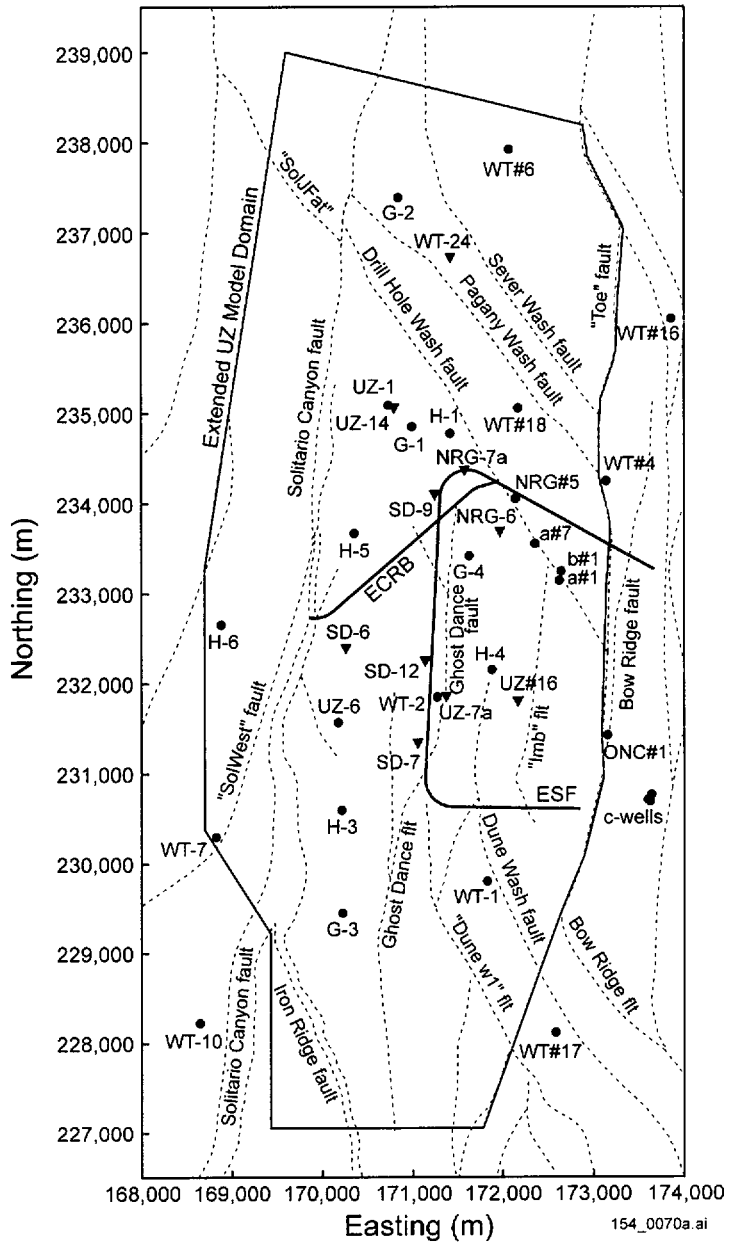

154_0070a.ai

Source: CRWMS M&O 2000 [DIRS 138860].

NOTE: Triangles represent wells from which qualified hydrogeologic rock property data were collected. Circles and triangles represent wells used to develop the geologic framework model. Dotted lines indicate fault traces per Geologic Framework Model version 3.1. Nevada coordinates in meters. ECRB = Enhanced Characterization of the Repository Block; ESF = Exploratory Studies Facility; UZ = unsaturated zone.

Figure 3.3.4-8. Data Locations Characterizing Repository Host Horizon Layers

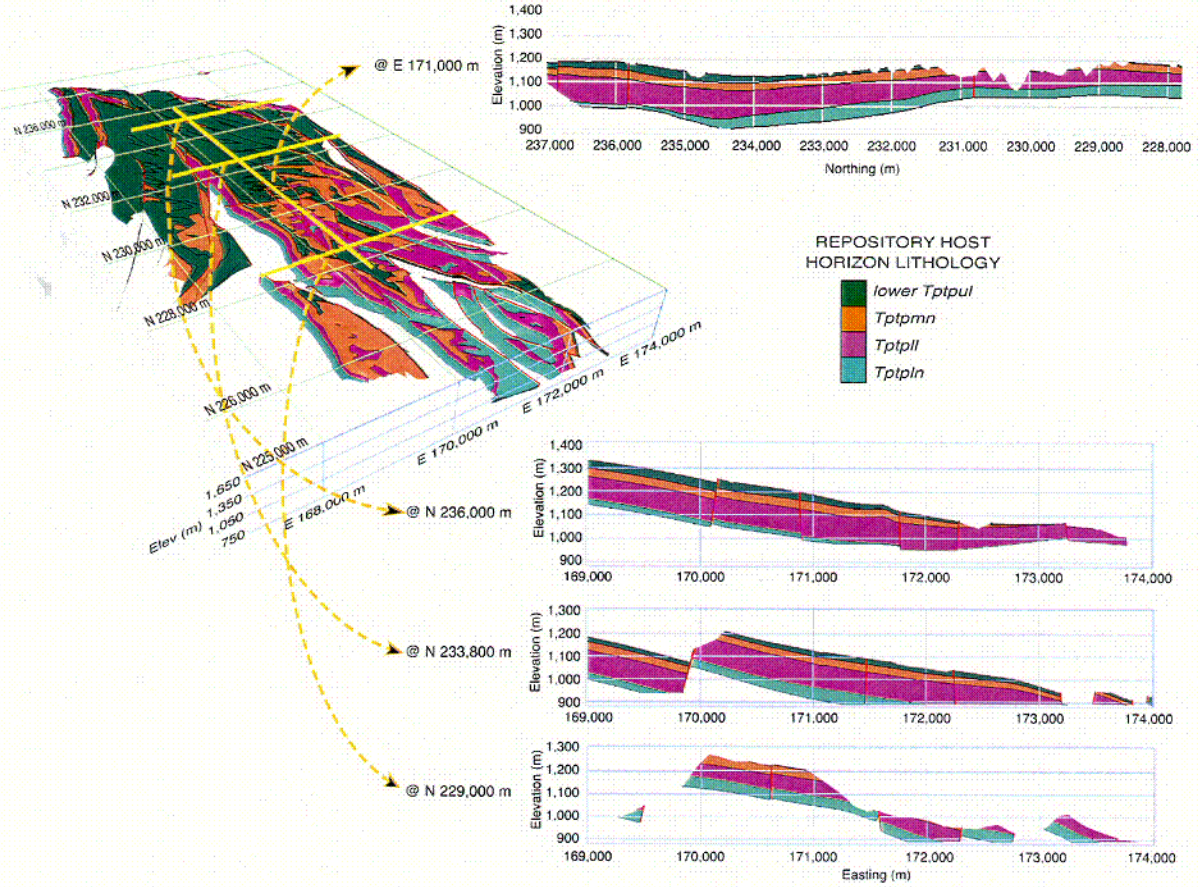

154_0071.ai

Source: Developed from DTN: MO9901MWDGFM31.000 [DIRS 103769].

NOTE: Upper and lower repository host horizon surfaces have been clipped to maintain an overburden thickness of 200 m and a water table standoff distance of 160 m. Nevada coordinates in meters.

Figure 3.3.4-9. Spatial Distribution of Lithostratigraphic Layers Constituting the Potential Repository Host Horizon

C16

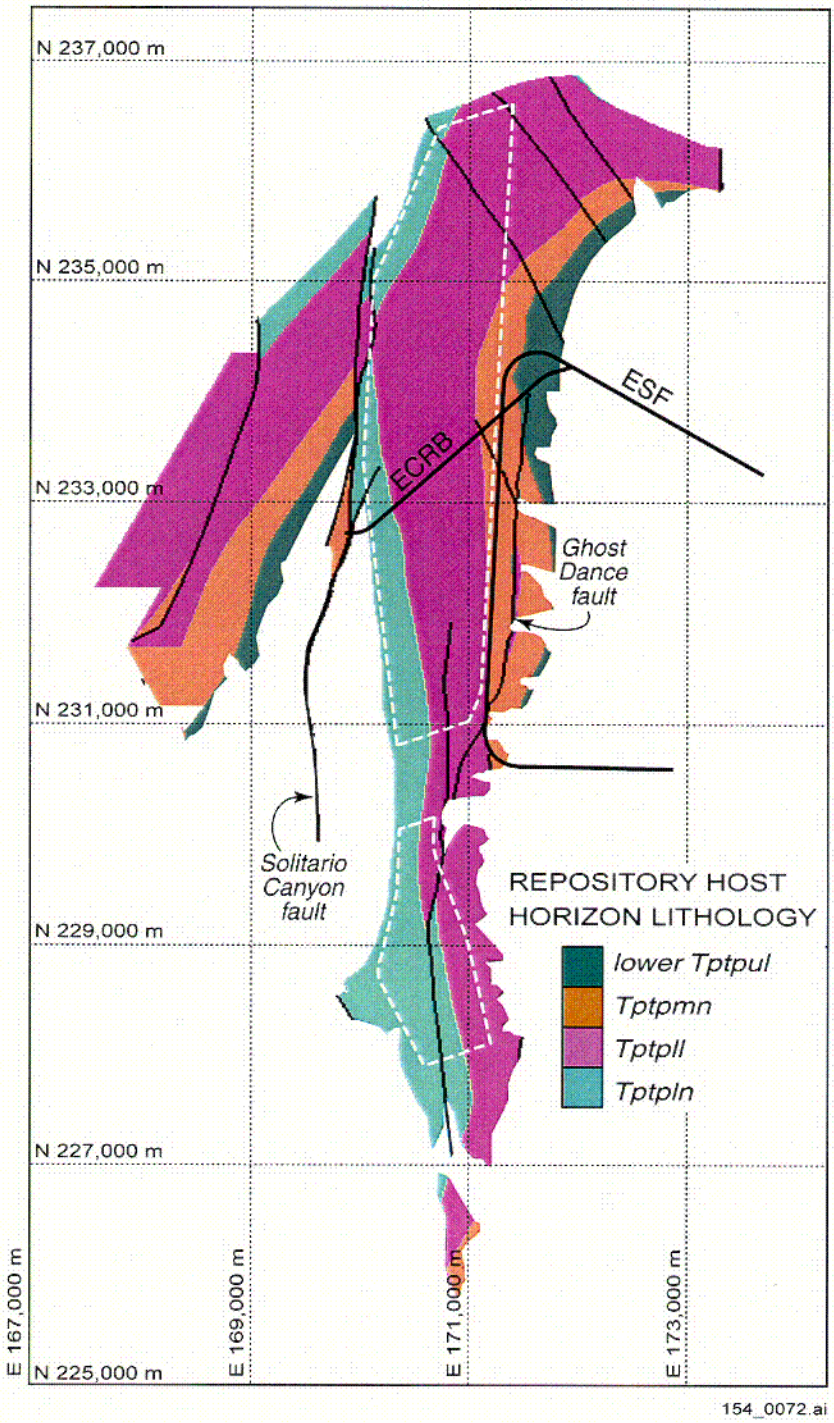

154_0072.ai

Source: Distribution of lithology from DTN: MO9901MWDGFM31.000 [DIRS 103769]. Design from BSC 2001 [DIRS 154548].

NOTE: The white dashed line identifies the plane of the current draft repository design. Nevada coordinates in meters. ECRB = Enhanced Characterization of the Repository Block; ESF = Exploratory Studies Facility; UZ = unsaturated zone.

Figure 3.3.4-10. Section Cut through the Potential Repository Siting Volume

C17

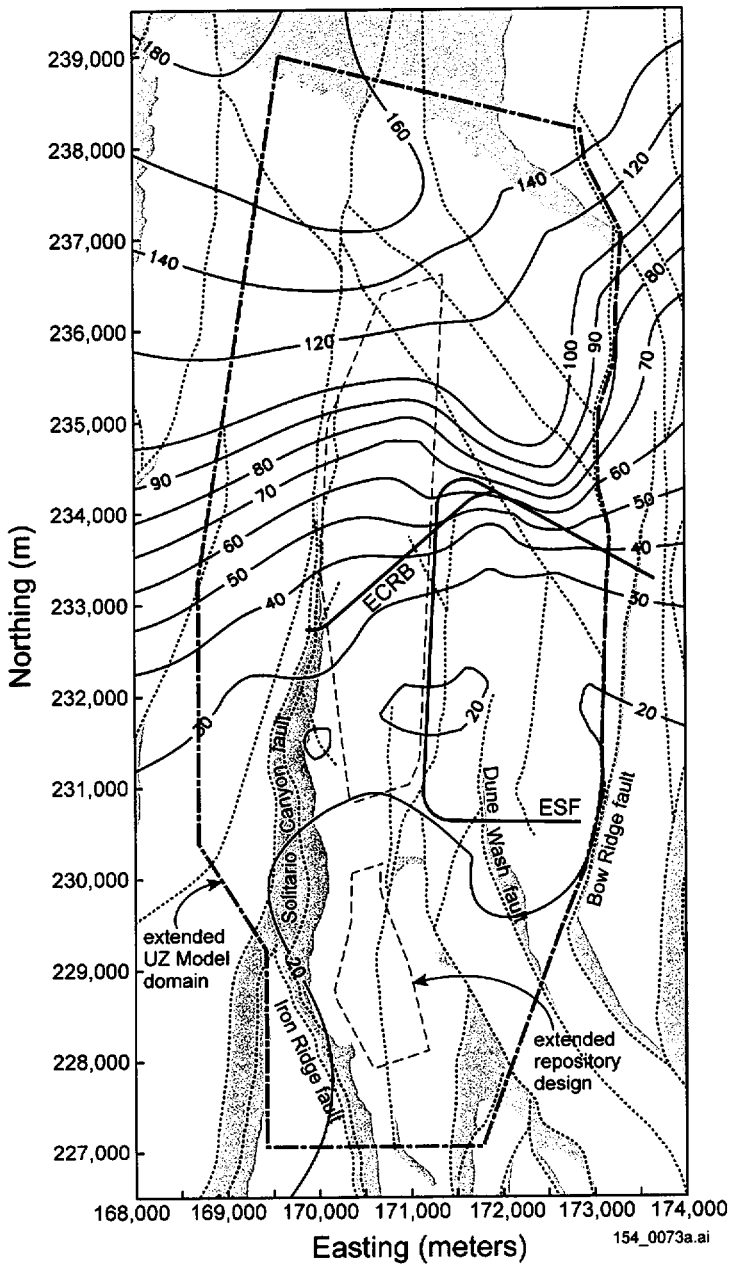

154_0073a.ai

Source: DTN: MO9901MWDGFM31.000 [DIRS 103769].

NOTE: Figure developed using Geologic Framework Model version 3.1 data. Contours indicate pre-faulted, pre-eroded PTn thickness in meters. Shaded areas are where the PTn has zero thickness as a result of faulting, erosion, or both. Nevada coordinates in meters. ECRB = Enhanced Characterization of the Repository Block; ESF = Exploratory Studies Facility; UZ = unsaturated zone.

Figure 3.3.4-11. PTn Occurrence and Thickness

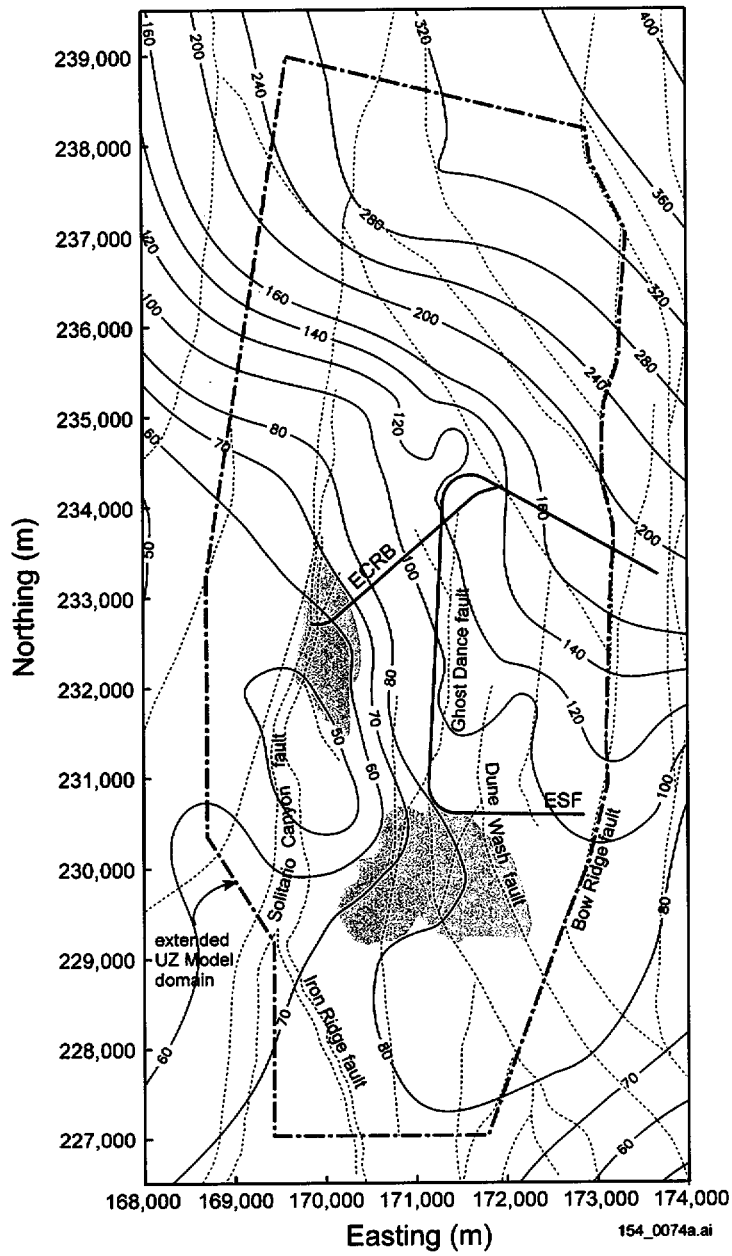

154_0074a.ai

Source: Thickness contours DTN: MO9901MWDGFM31.000 [DIRS 103769]. Vitric extent estimated using preliminary RPM3.2 data Bodvarsson 2001 [DIRS 154669], Attachment 15, pp. 148 to 151.

NOTE: Thickness contours developed using Geologic Framework Model version 3.1 data. Units are meters. Shaded areas represent estimated extent of vitric region within the extended Unsaturated Zone model domain near the top of the CHn (light shading) and near the base of the CHn (dark shading). Nevada coordinates in meters. ECRB = Enhanced Characterization of the Repository Block; ESF = Exploratory Studies Facility; UZ = unsaturated zone.

Figure 3.3.4-12. Pre-faulted, Pre-eroded Thickness Map of CHn (Tptpv1–Tacbt)

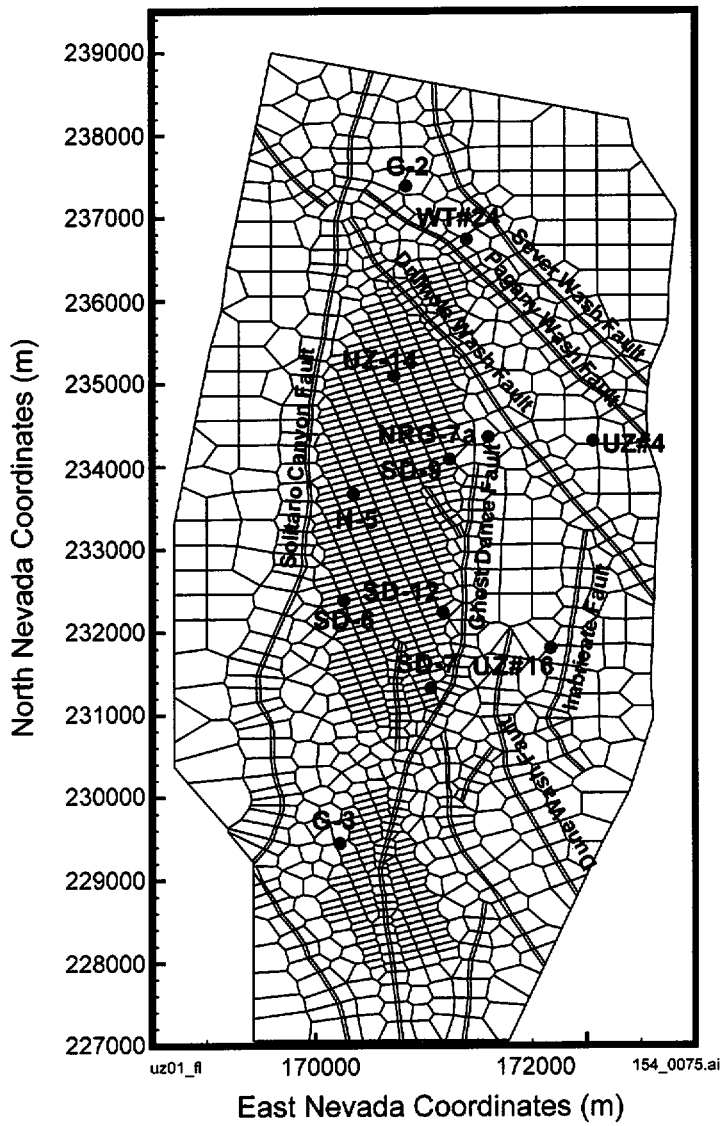

154_0075.ai

Source: BSC 2001 [DIRS 154548].

NOTE: Shown are modeled faults, several borehole locations, and refinements in the potential repository area (using the extended design for a cooler repository).

Figure 3.3.4-13. Plan View of the Extended Model Grid

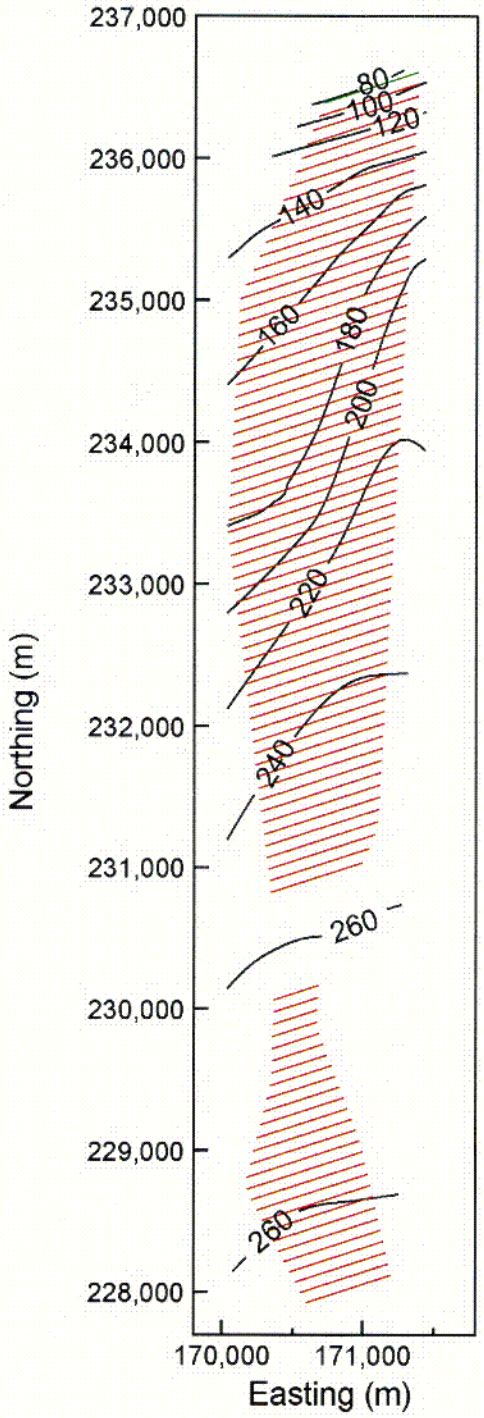

154_0528.ai

Source: Layout of the potential repository emplacement drifts from BSC (2001 [DIRS 154548], Item 1 of Figure 1 and Table 1).

NOTE: Contours in meters. Red lines indicate emplacement drifts. The northernmost drift (green) is a post-closure test drift.

Figure 3.3.4-13a. Approximate Vertical Distance Between Emplacement Drifts and a Water Table 120 m Above the Current Elevation

C18

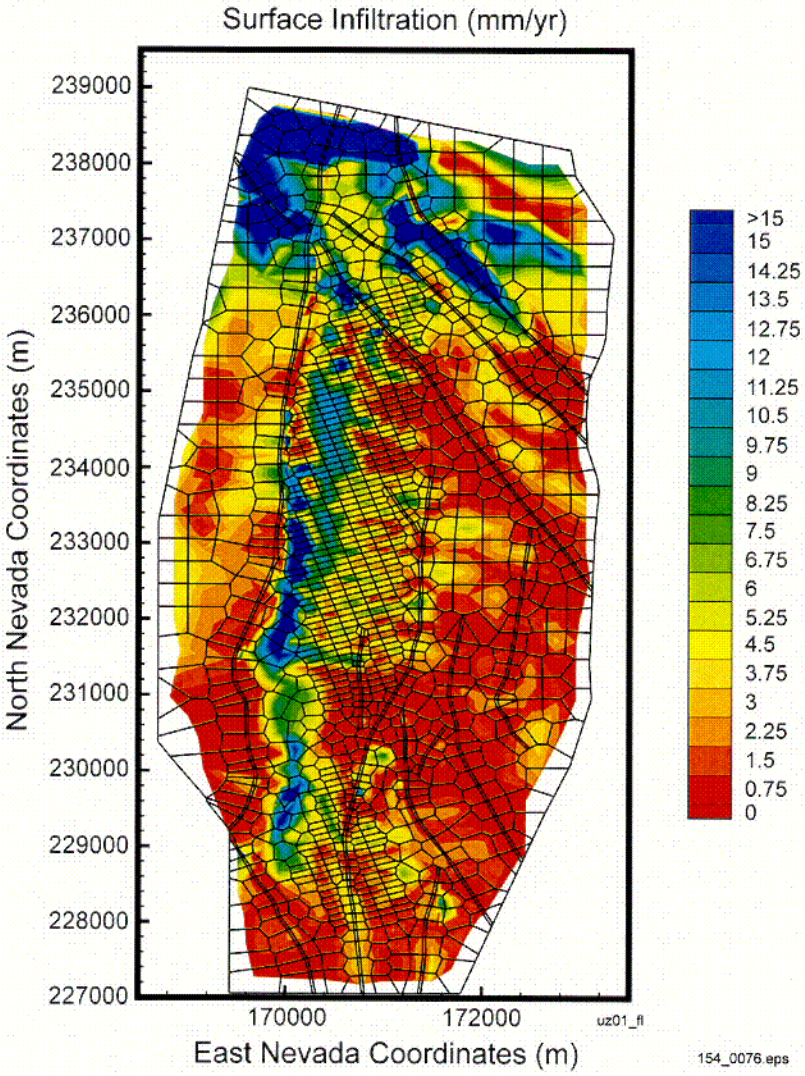

154_0076.eps

Source: Preliminary work described by Bodvarsson 2001 [DIRS 154669], Attachment 13, p. 13.

NOTE: Simulation uses present-day, mean infiltration (mm/yr).

Figure 3.3.4-14. Spatial Distribution of Infiltration in the Domain of the Extended Model

C19

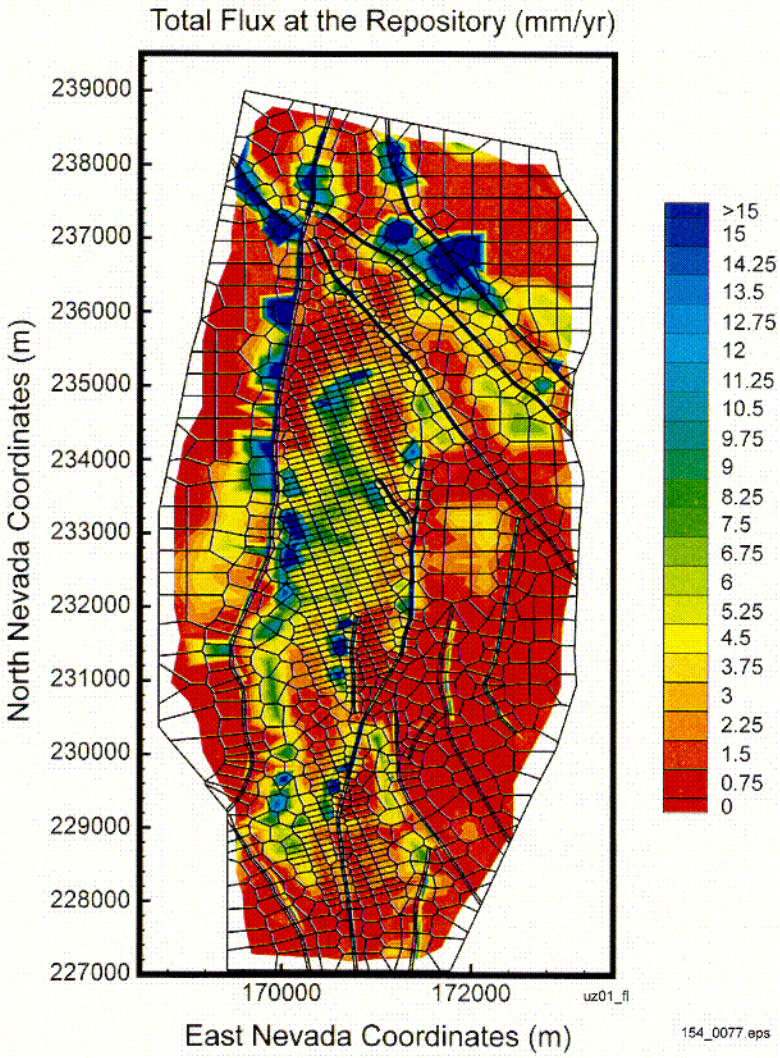

154_0077.eps

Source: Preliminary work described by Bodvarsson 2001 [DIRS 154669], Attachment 13, p. 15.

NOTE: Simulation uses present-day, mean infiltration (mm/yr).

Figure 3.3.4-15. Simulated Percolation Flux at the Potential Repository Horizon Using the Extended Model Grid

C20

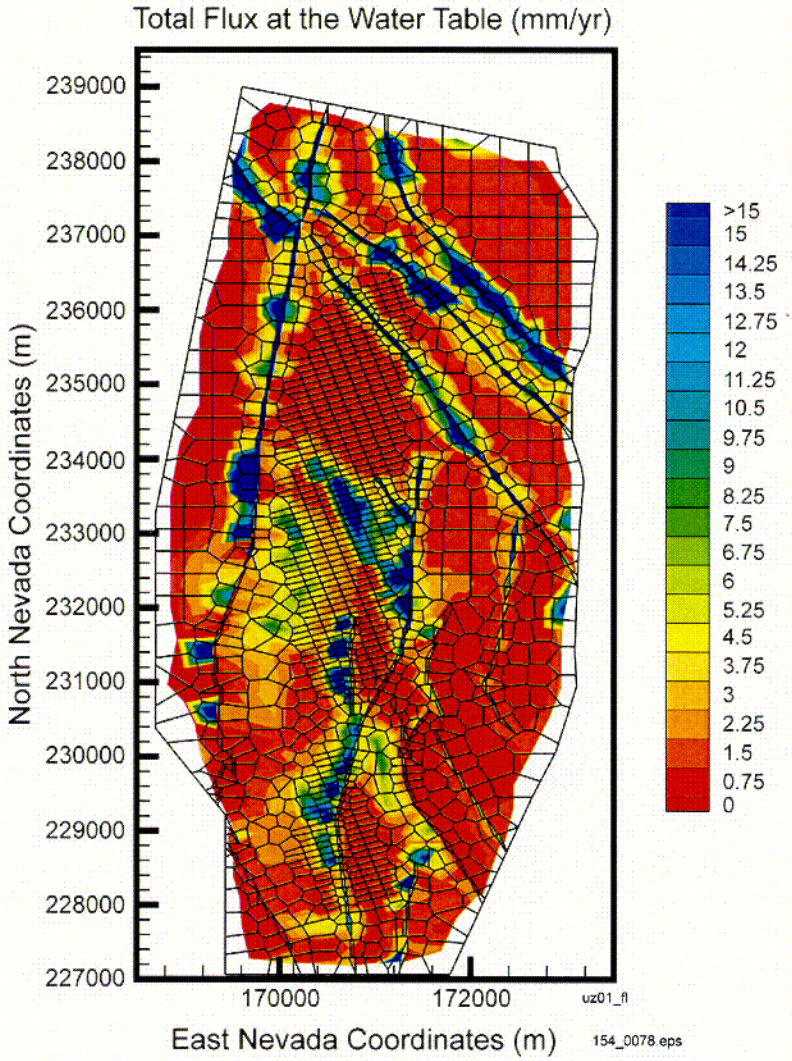

154_0078.eps

Source: Preliminary work described by Bodvarsson 2001 [DIRS 154669], Attachment 13, p. 16.

NOTE: Simulation uses present-day, mean infiltration (mm/yr).

Figure 3.3.4-16. Simulated Percolation Flux at the Water Table Using the Extended Model Grid

C21

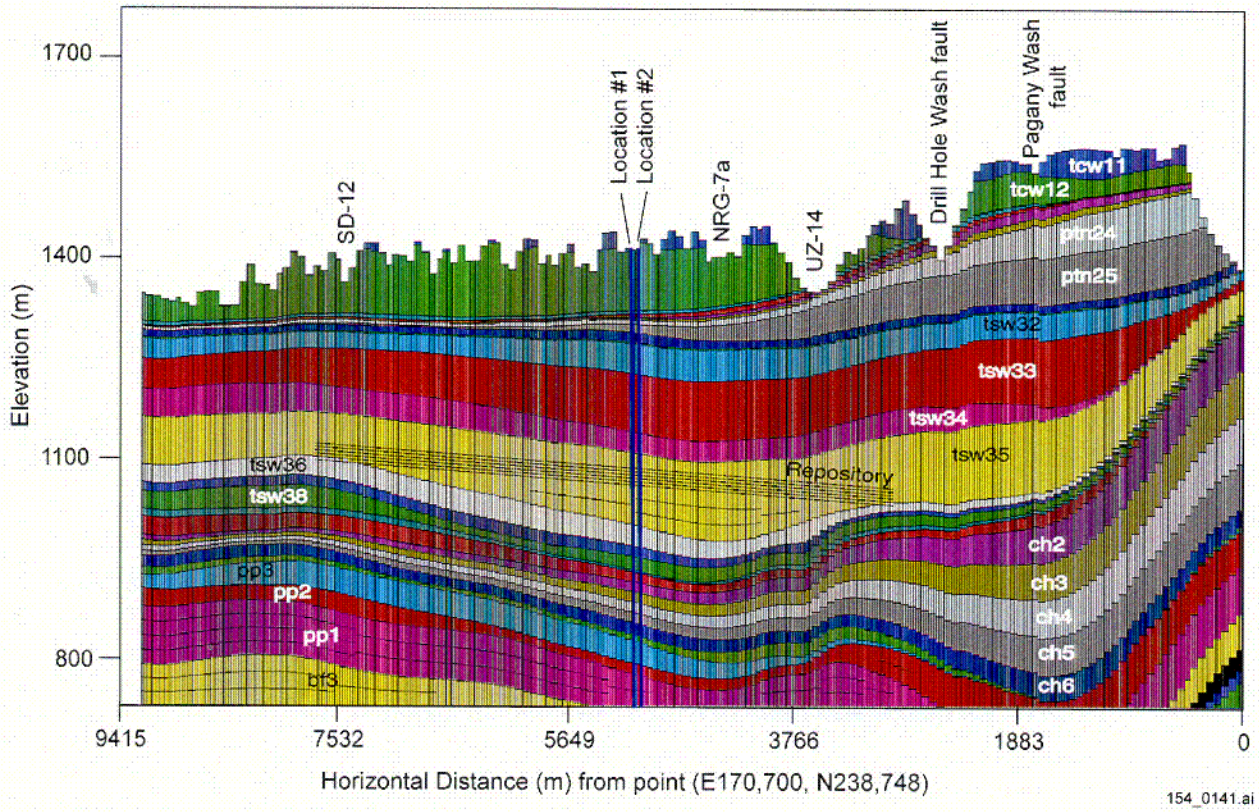

154_0141.ai

Source: CRWMS M&O 2000 [DIRS 144454], Figure 3.

NOTE: Lateral and vertical discretization, two-dimensional NS#2 cross section based on the refined numerical grid.

Figure 3.3.5-1. Location of the Potential Repository and Layering of the Hydrogeologic Units

C22

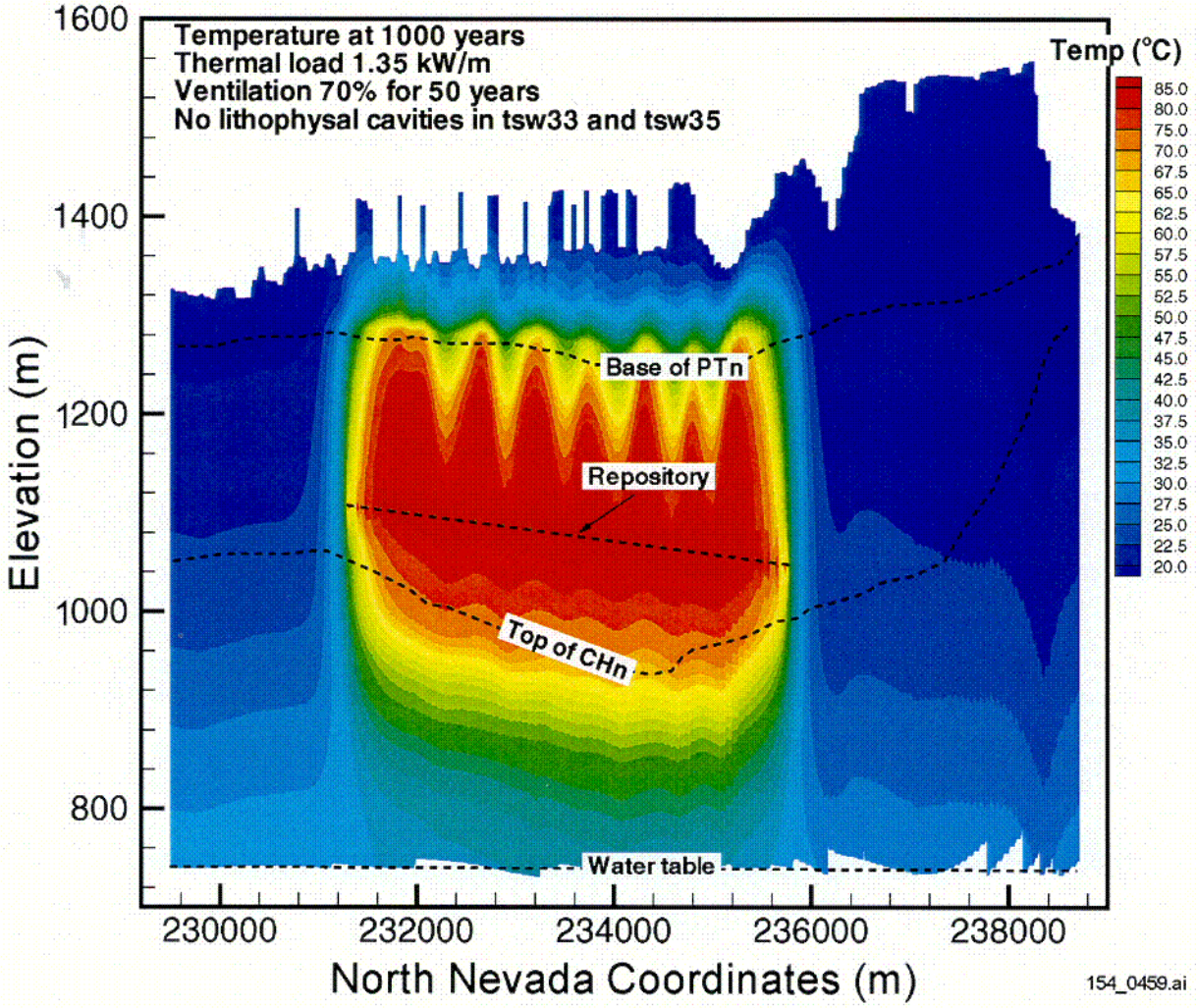

154_0459.ai

Source: Bodvarsson 2001 [DIRS 154669], Attachment 10, p. 11.

NOTE: Case #3: thermal load = 1.35 kW/m; ventilation = 70 percent for 50 years; no lithophysal cavities. Two-dimensional cross section.

Figure 3.3.5-2. Temperature Distribution for the Potential Higher-Temperature Repository at 1,000 Years

C23

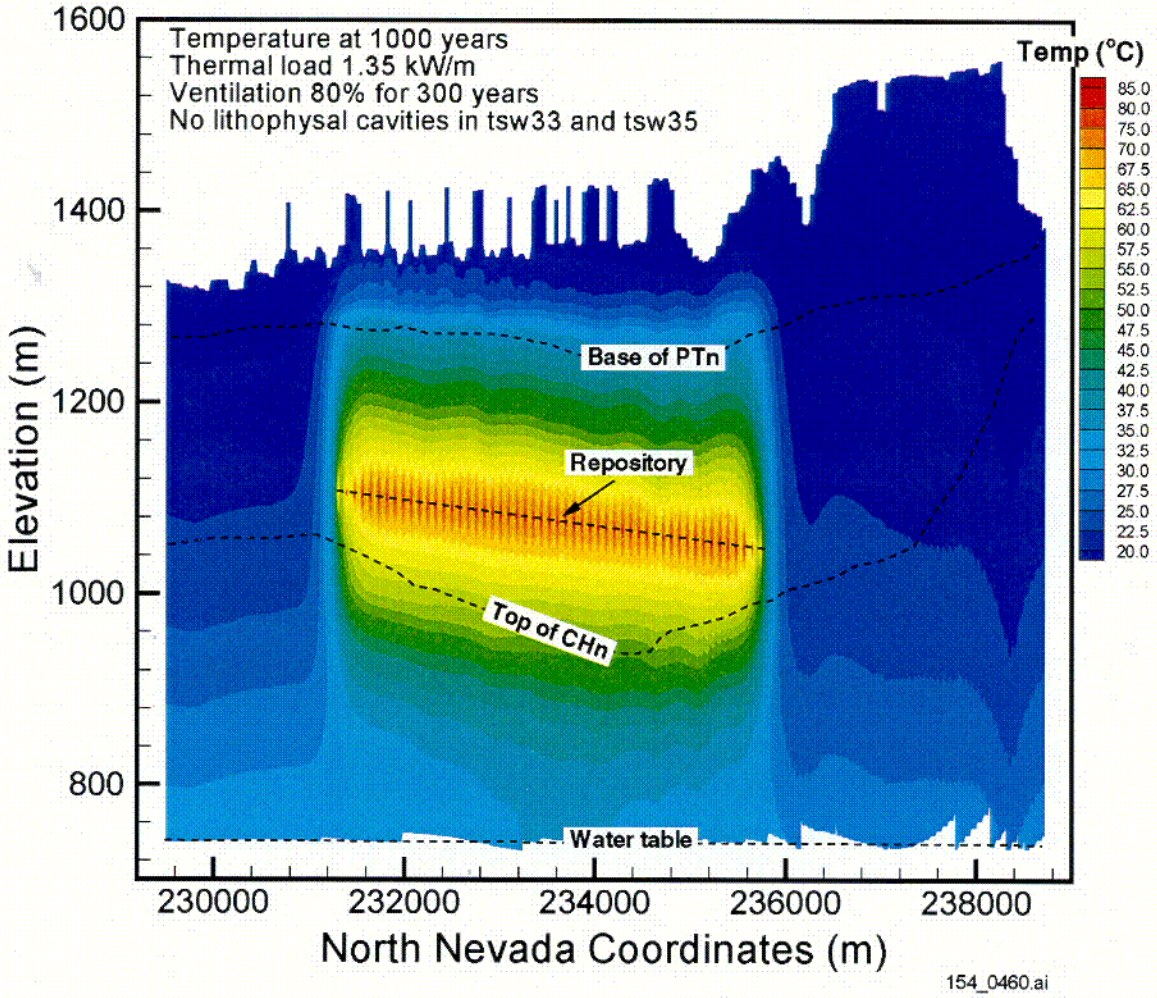

154_0460.ai

Source: Bodvarsson 2001 [DIRS 154669], Attachment 6, p. 101.

NOTE: Case #5: thermal load = 1.35 kW/m; ventilation = 80 percent for 300 years; no lithophysal cavities. Two-dimensional cross section.

Figure 3.3.5-3. Temperature Distribution for the Potential Lower-Temperature Repository at 1,000 Years

C24

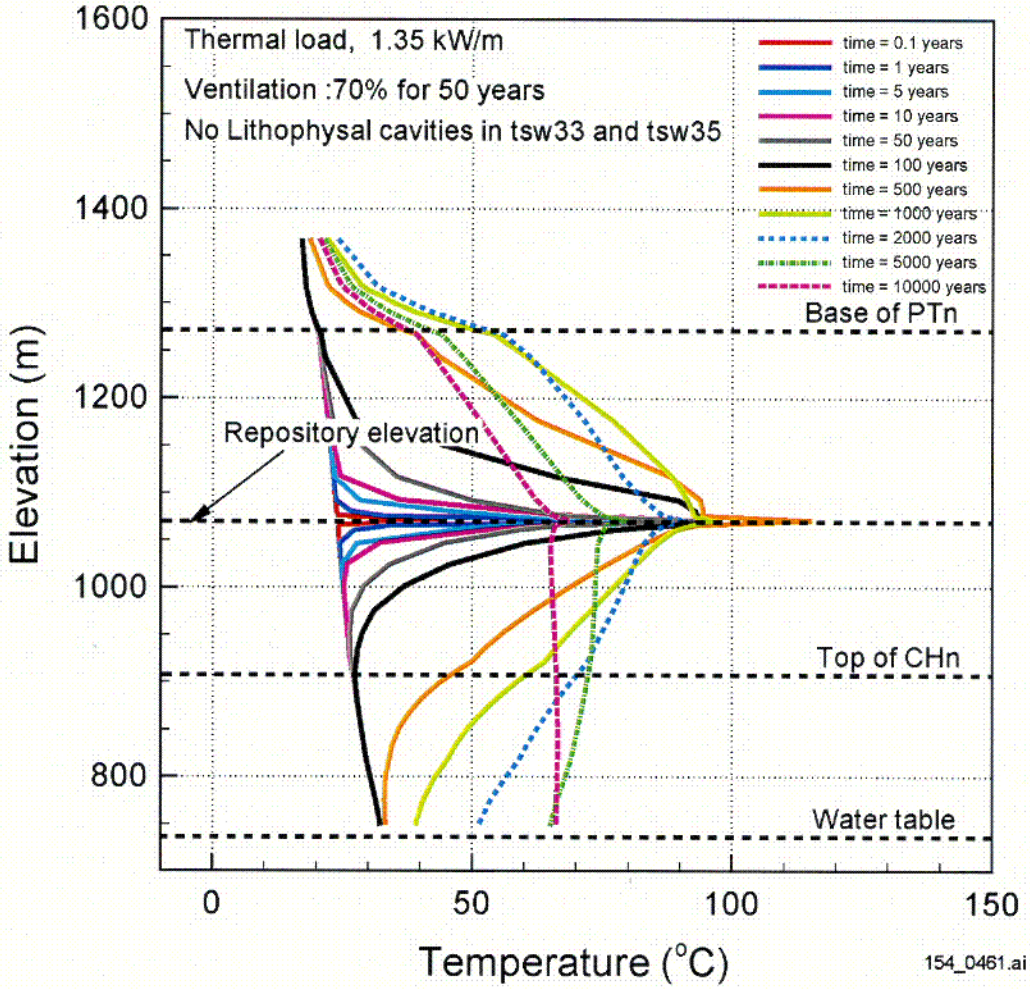

154_0461.ai

Source: Bodvarsson 2001 [DIRS 154669], Attachment 6, p. 83.

NOTE: Case #3: thermal load = 1.35 kW/m; ventilation = 70 percent for 50 years; no lithophysal cavities in tsw33 and tsw35. Two-dimensional cross section.

Figure 3.3.5-4. Temperature Profiles at the Center of the Potential Higher-Temperature Repository, No Lithophysal Cavities

C25

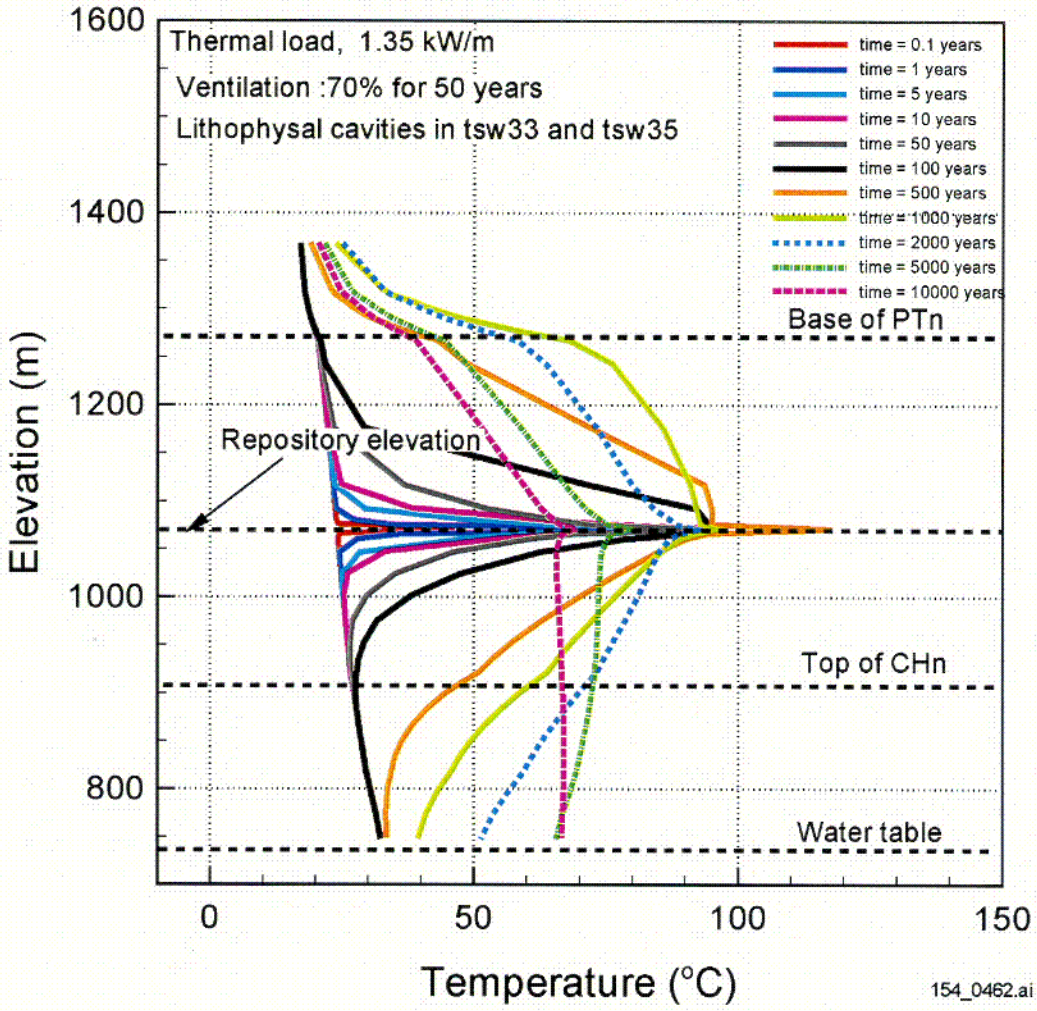

154_0462.ai

Source: Bodvarsson 2001 [DIRS 154669], Attachment 6, p. 84.

NOTE: Case #4: thermal load = 1.35 kW/m; ventilation = 70 percent for 50 years; with lithophysal cavities in tsw33 and tsw35. Two-dimensional cross section.

Figure 3.3.5-5. Temperature Profiles at the Center of the Potential Higher-Temperature Repository, with Lithophysal Cavities

C26

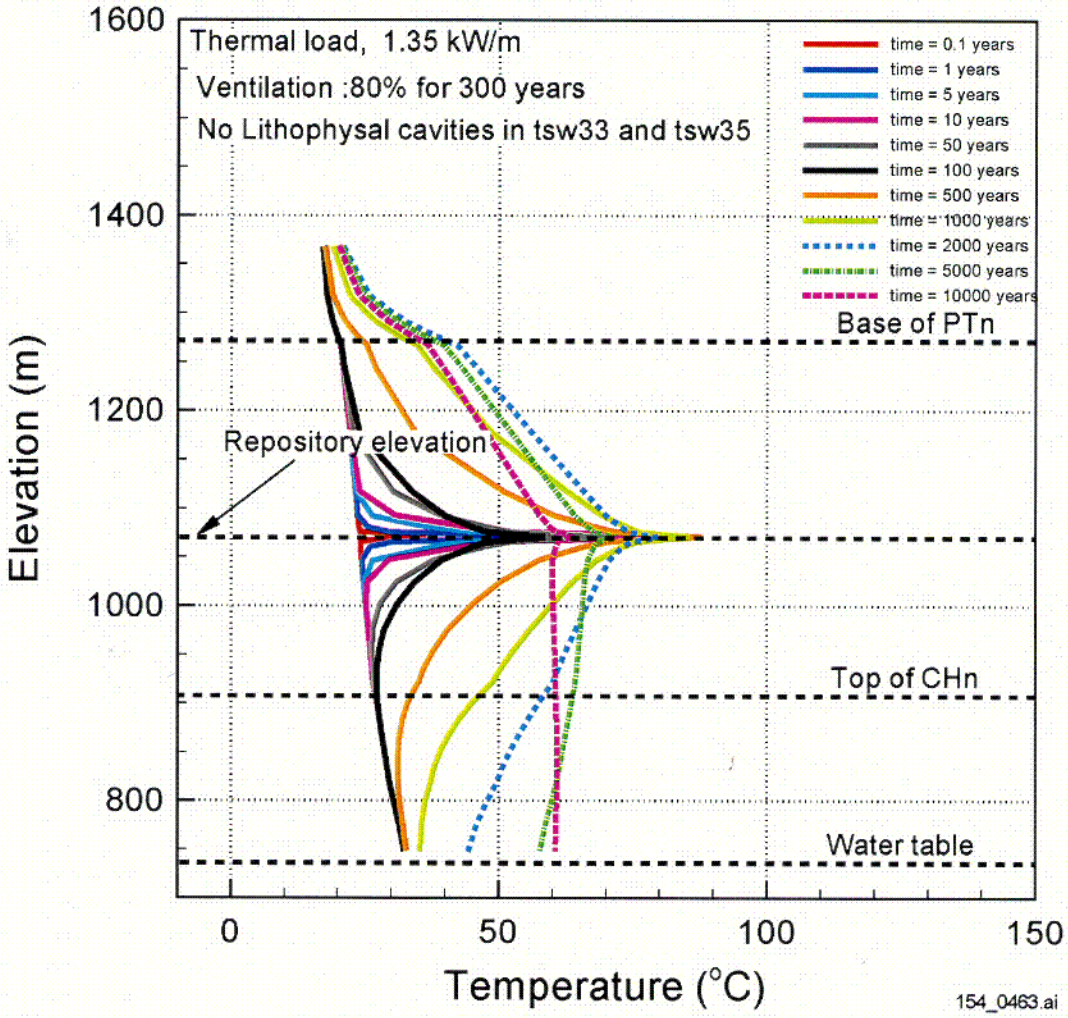

154_0463.ai

Source: Bodvarsson 2001 [DIRS 154669], Attachment 6, p. 85.

NOTE: Case #5: thermal load = 1.35 kW/m; ventilation = 80 percent for 300 years; no lithophysal cavities in tsw33 and tsw35. Two-dimensional cross section.

Figure 3.3.5-6. Temperature Profiles at the Center of the Potential Lower-Temperature Repository, No Lithophysal Cavities

C27

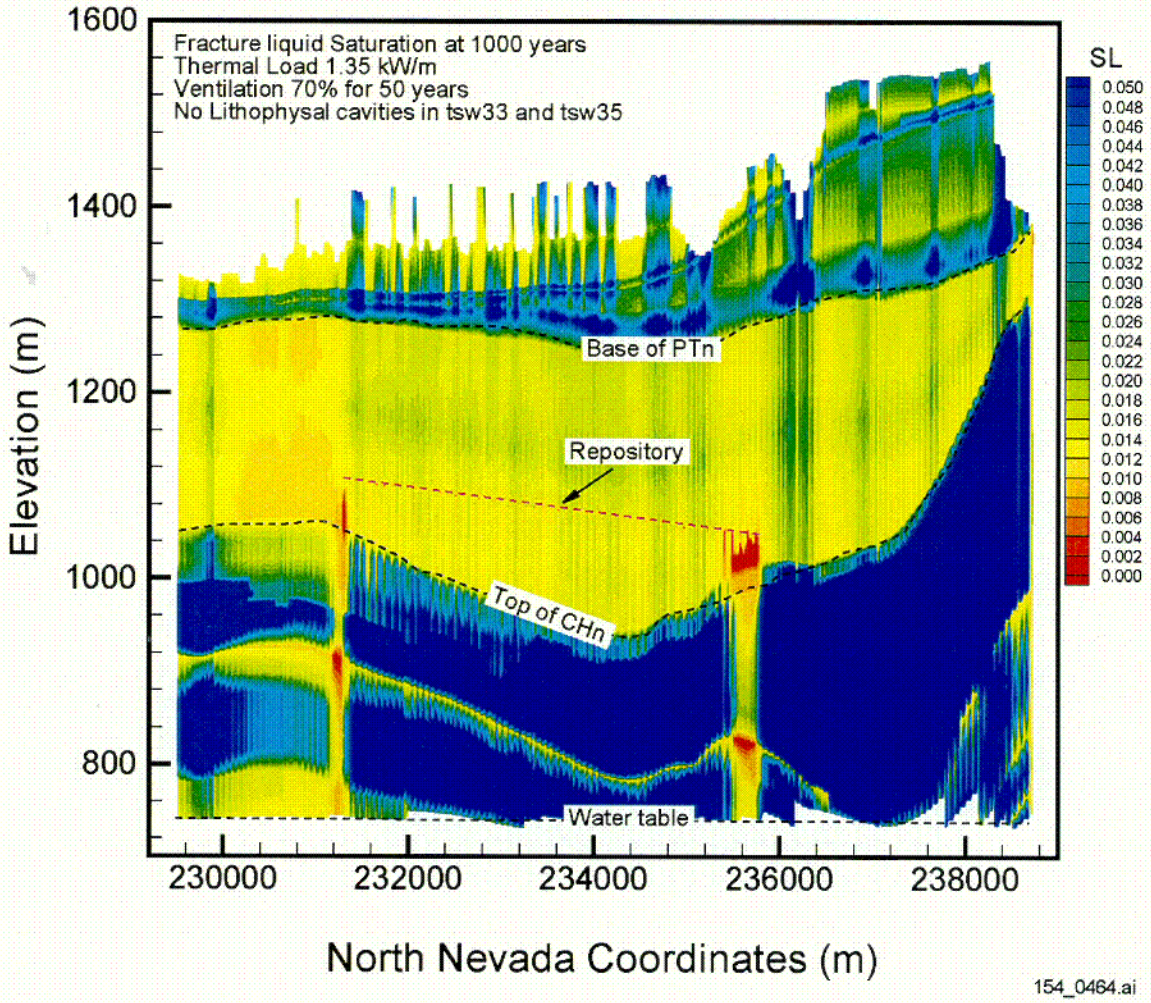

154_0464.ai

Source: Bodvarsson 2001 [DIRS 154669], Attachment 6, p. 100.

NOTE: Case #3: thermal load = 1.35 kW/m; ventilation = 70 percent for 50 years; no lithophysal cavities. Two-dimensional cross section.

Figure 3.3.5-7. Fracture Liquid Saturation for the Potential Higher-Temperature Repository at 1,000 Years

C28

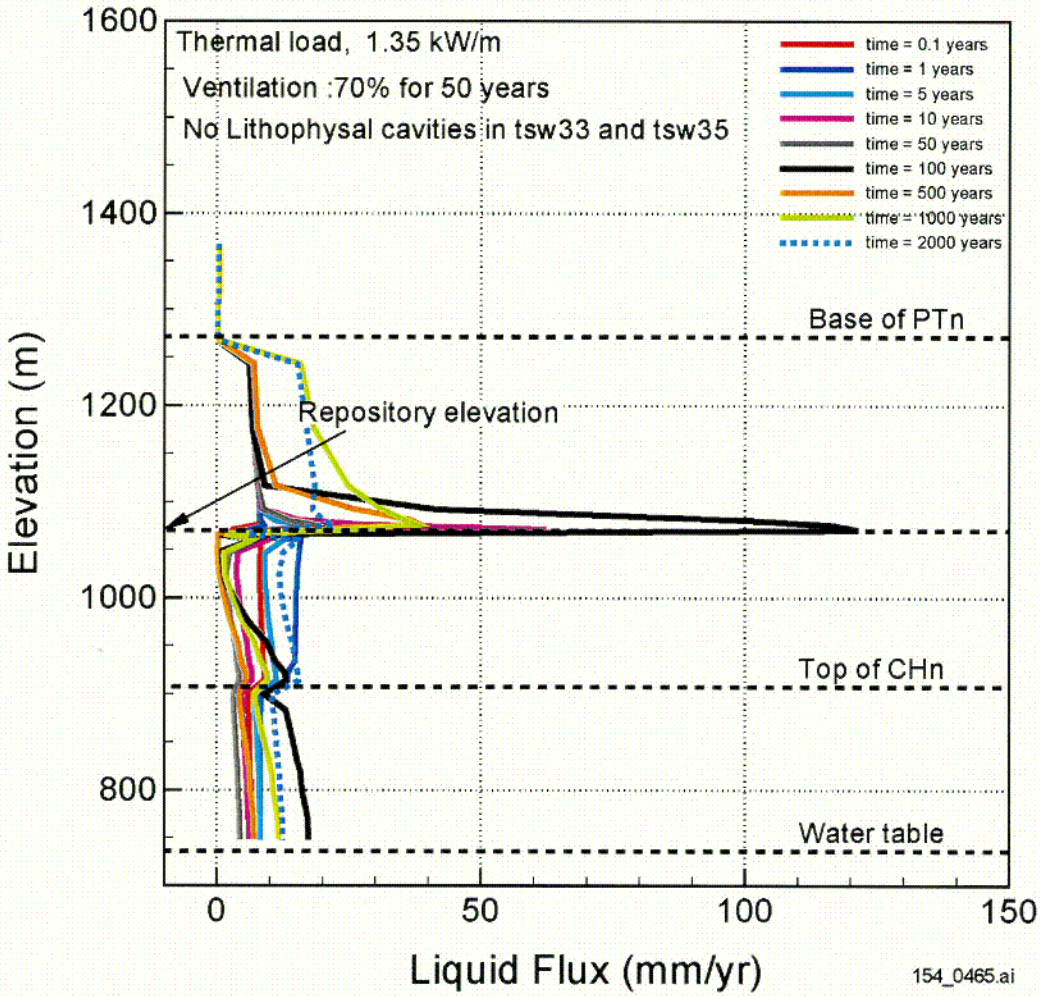

154_0465.ai

Source: Bodvarsson 2001 [DIRS 154669], Attachment 6, p. 91.

NOTE: Case #3: thermal load = 1.35 kW/m; ventilation = 70 percent for 50 years; no lithophysal cavities in tsw33 and tsw35. Two-dimensional cross section.

Figure 3.3.5-8. Fracture Liquid-Flux Profiles at Center of the Potential Repository for the Higher-Temperature Repository, No Lithophysal Cavities

C29

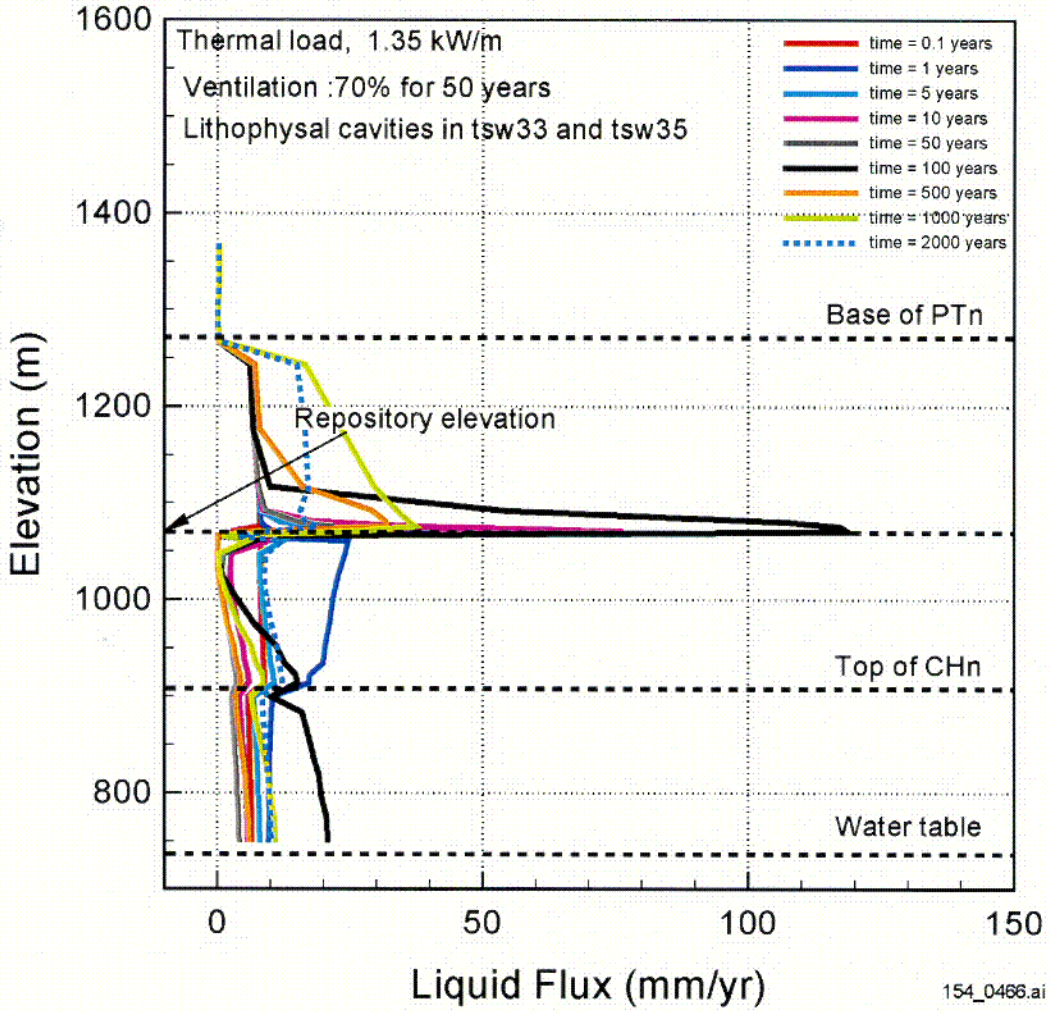

154_0466.ai

Source: Bodvarsson 2001 [DIRS 154669], Attachment 6, p. 92.

NOTE: Case #4: thermal load = 1.35 kW/m; ventilation = 70 percent for 50 years; with lithophysal cavities in tsw33 and tsw35. Two-dimensional cross section.

Figure 3.3.5-9. Fracture Liquid Flux Profiles at the Center of the Potential Higher-Temperature Repository, With Lithophysal Cavities

C30

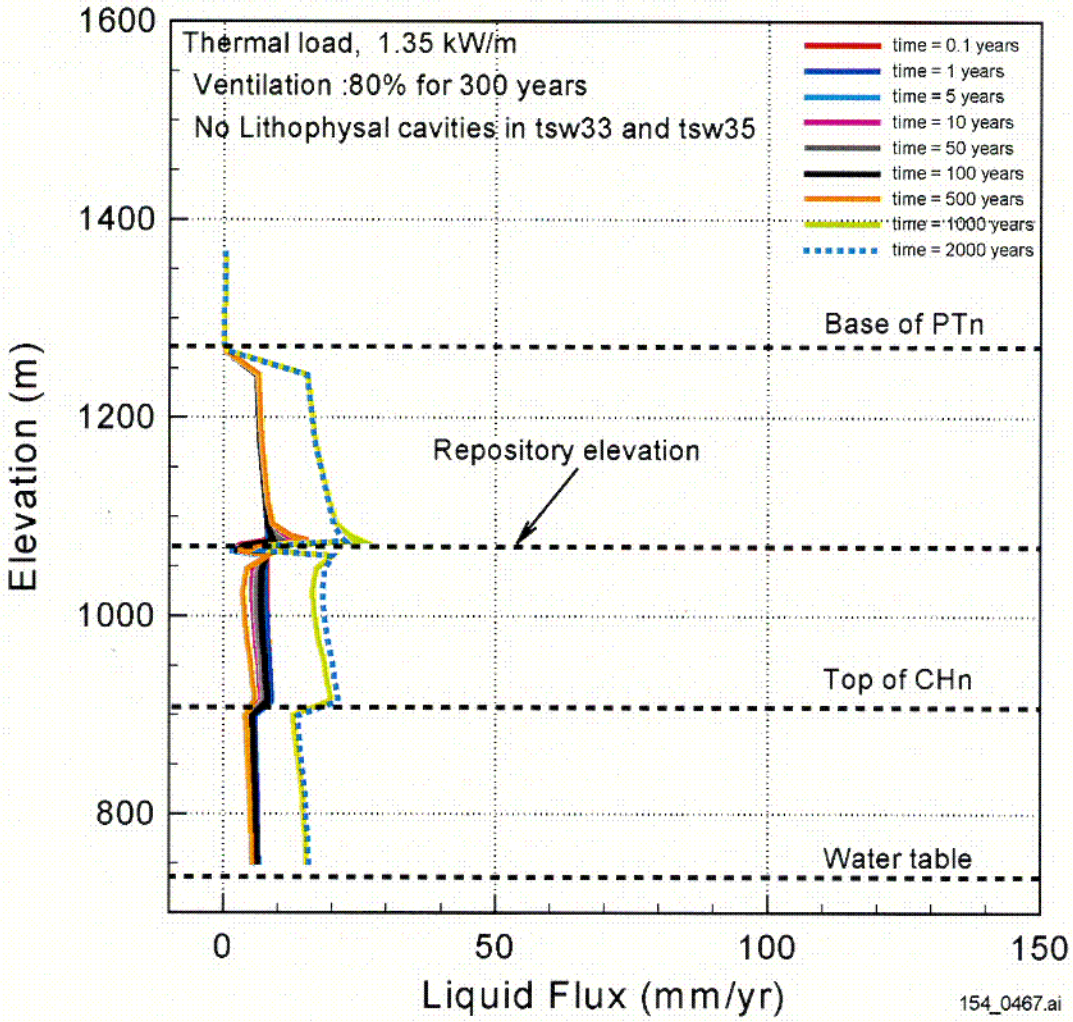

154_0467.ai

Source: Bodvarsson 2001 [DIRS 154669], Attachment 6, p. 93.

NOTE: Case #5: thermal load = 1.35 kW/m; ventilation = 80 percent for 300 years; no lithophysal cavities in tsw33 and tsw35. Two-dimensional cross section.

Figure 3.3.5-10. Fracture Liquid Flux Profiles at the Center of the Potential Lower-Temperature Repository, No Lithophysal Cavities

C31

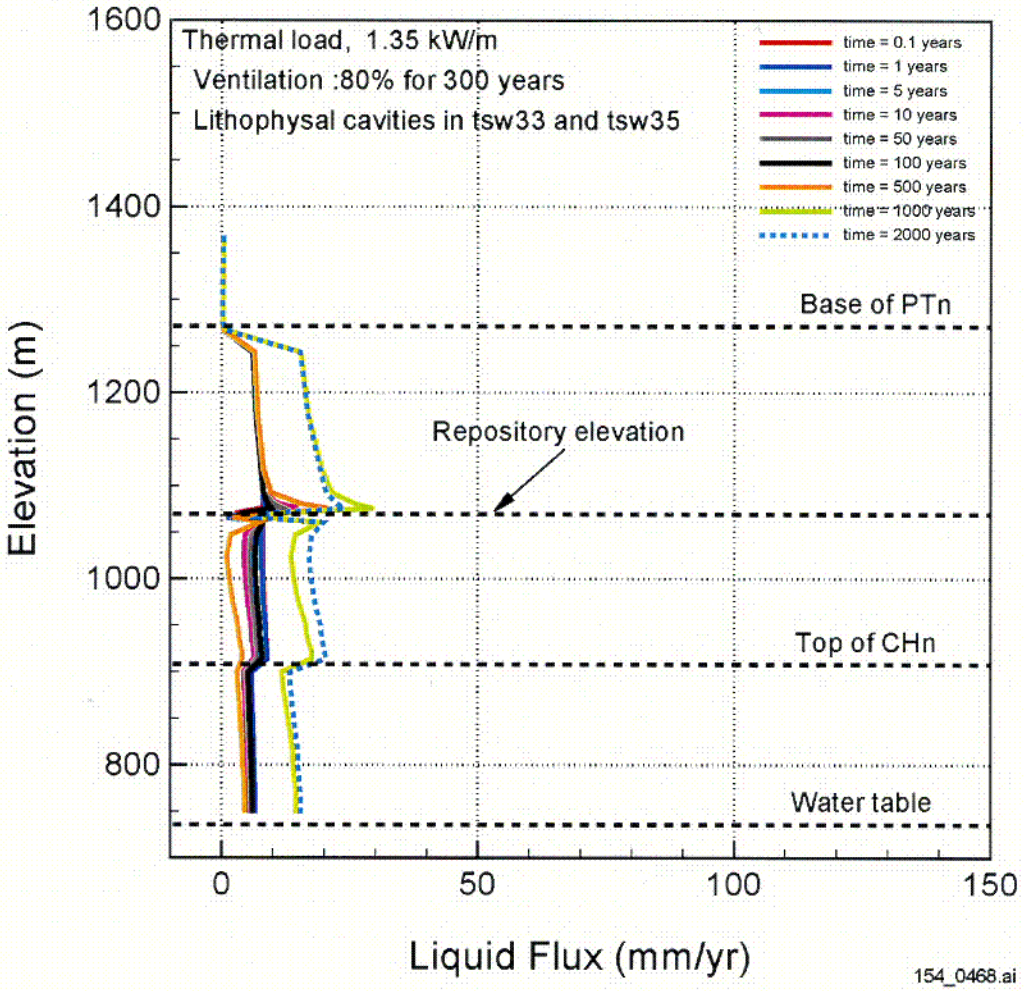

154_0468.ai

Source: Bodvarsson 2001 [DIRS 154669], Attachment 6, p. 94.

NOTE: Case #6: thermal load = 1.35 kW/m; ventilation = 80 percent for 300 years; with lithophysal cavities in tsw33 and tsw35. Two-dimensional cross section.

Figure 3.3.5-11. Fracture Liquid-Flux Profiles at the Center of the Potential Lower-Temperature Repository, With Lithophysal Cavities

C32

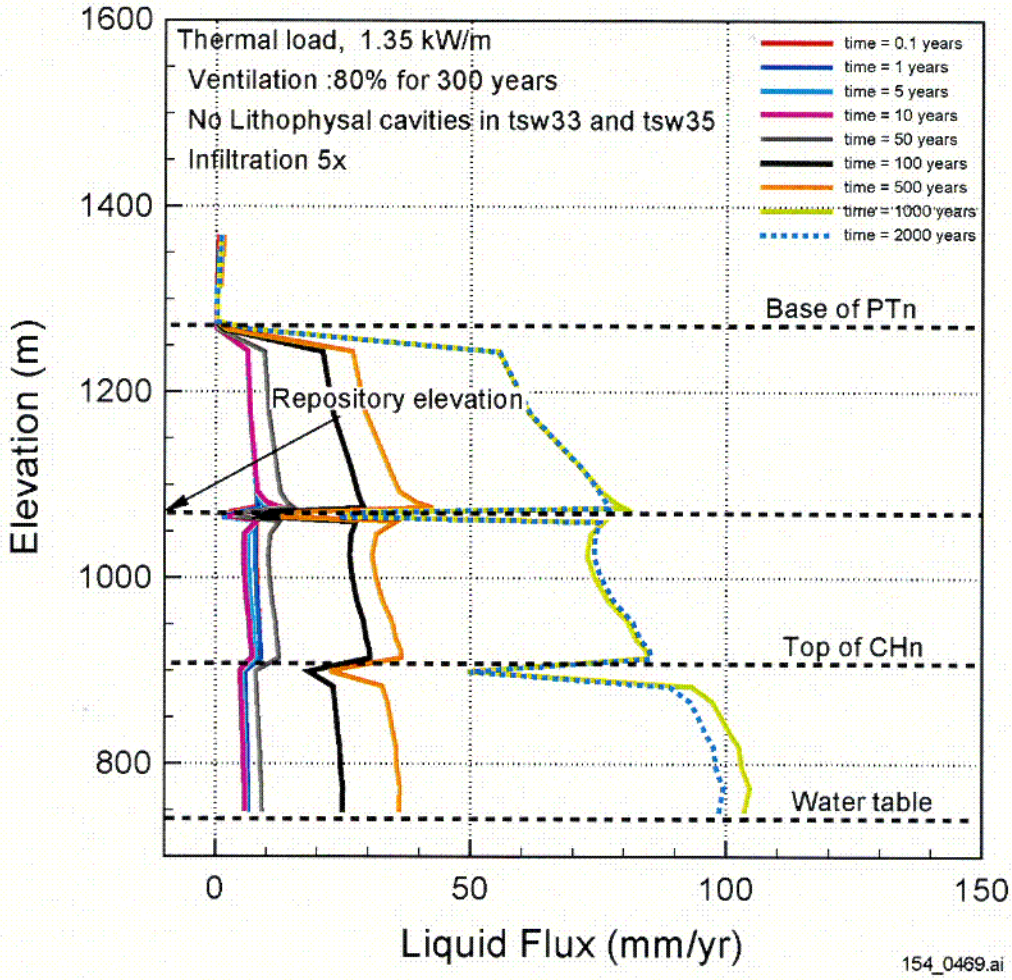

154_0469.ai

Source: Bodvarsson 2001 [DIRS 154669], Attachment 6, p. 103.

NOTE: Case #7: thermal load = 1.35 kW/m; ventilation = 80 percent for 300 years; no lithophysal cavities in tsw33 and tsw35. Two-dimensional cross section.

Figure 3.3.5-12. Fracture Liquid Flux Profiles at the Center of the Potential Lower-Temperature Repository, No Lithophysal Cavities and Increased Infiltration

C33

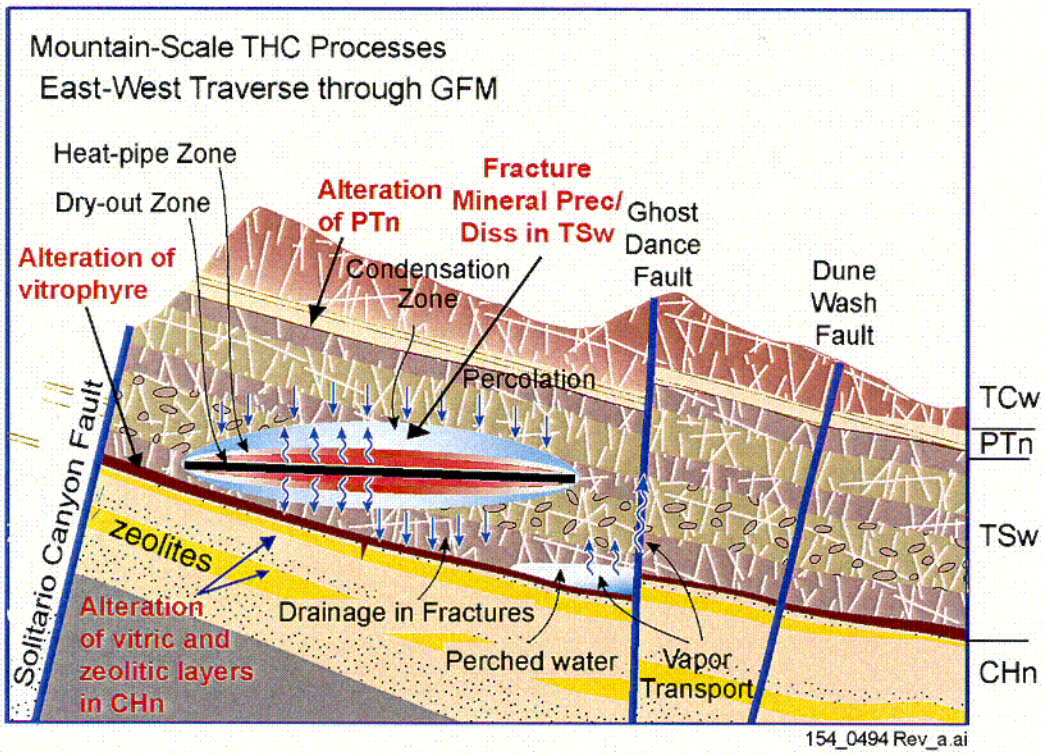

154_0494 Rev_a.ai

NOTE: Definitions: GFM = Geologic Frame Model; TCw = Tiva Canyon welded hydrogeologic unit; PTn = Paintbrush Tuff nonwelded hydrogeologic unit; TSw = Topopah Spring welded hydrogeologic unit; CHn = Calico Hills nonwelded hydrogeologic unit.

Figure 3.3.6-1. Schematic of Potential Mountain-Scale Thermal-Hydrologic-Chemical Processes and Initial Conditions

C34

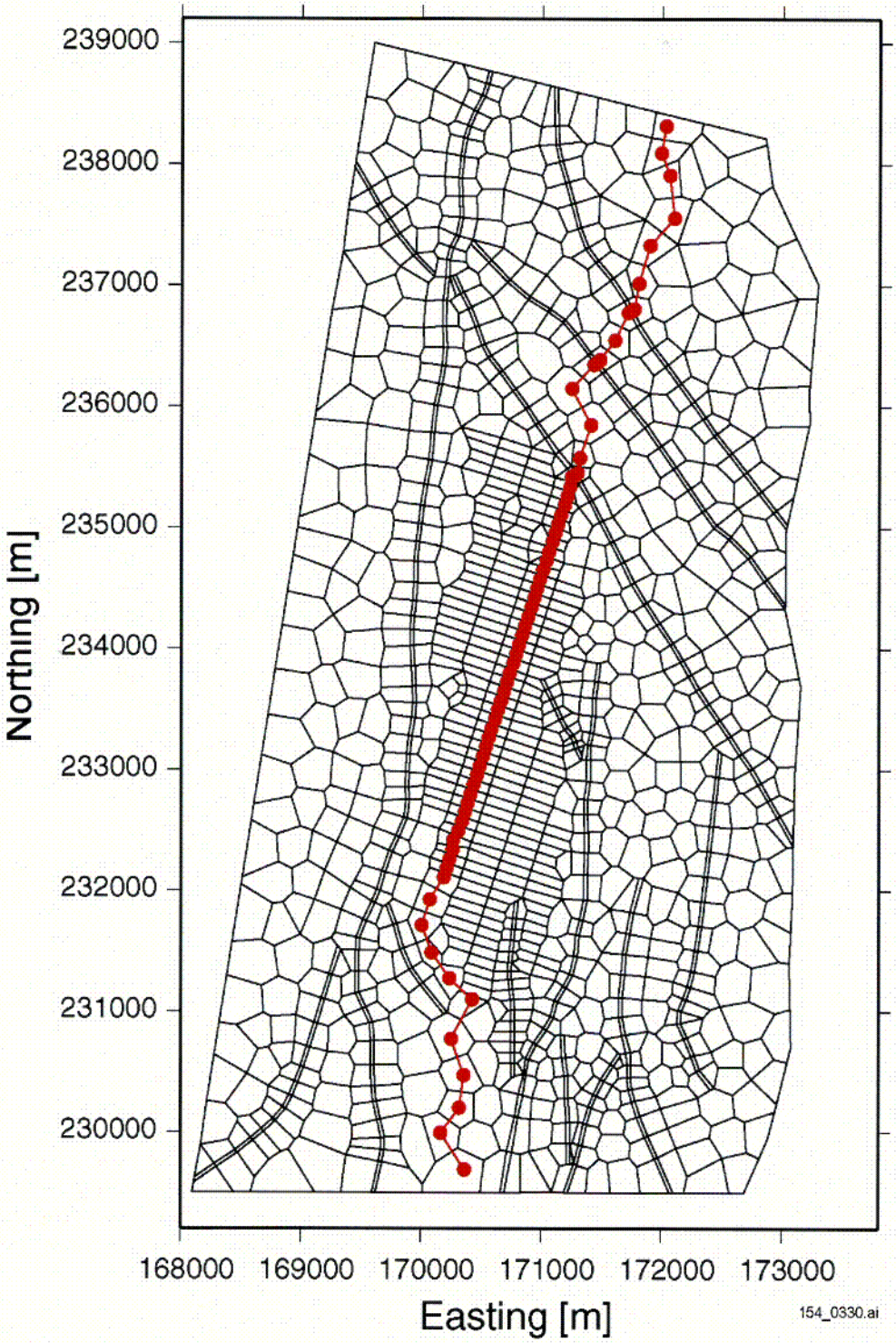

154_0330.ai

Source: Bodvarsson 2001 [DIRS 154669], Attachment 10, p. 11.

NOTE: Nevada Coordinates in meters.

Figure 3.3.6-2. Location of 2-D North-South Cross Section Superimposed on Diagram Showing the 3-D UZ Flow and Transport Model TSPA-SR Grid

C35

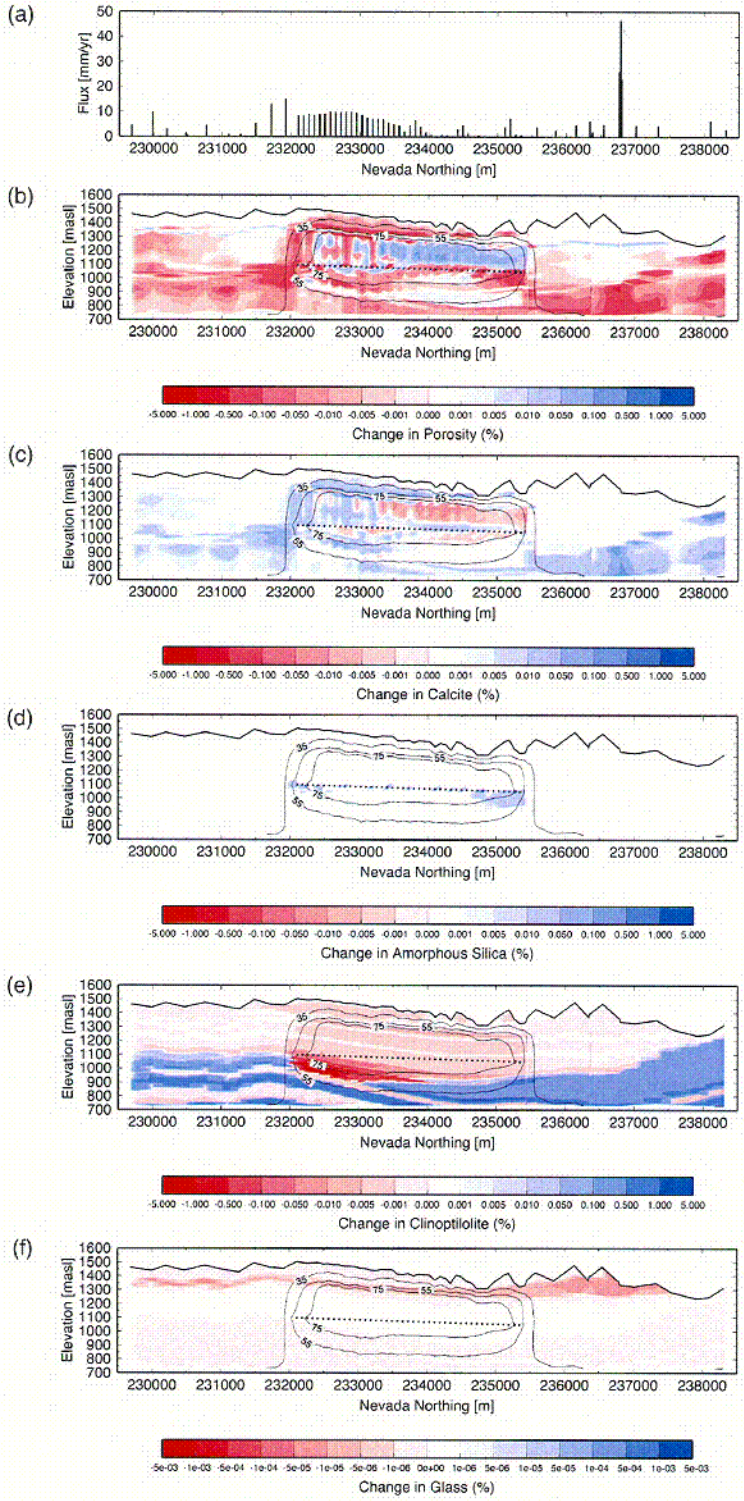

154_0254

Source: Bodvarsson 2001 [DIRS 154669], Attachment 10, pp. 12 to 14.

NOTE: Extended Case 1. Crosses denote model repository drift locations: (a) infiltration rate; (b) fracture porosity change with temperature contours; (c) fracture calcite change with temperature contours; (d) fracture amorphous silica precipitation with temperature contours; (e) matrix clinoptilolite change with temperature contours; and (f) matrix glass dissolution with temperature contours. masl = meters above sea level.

Figure 3.3.6-3. Infiltration Rate Distribution and Simulated Changes in Fracture Porosity, Mineralogy, and Temperature after about 1,400 Years of Heating

C36

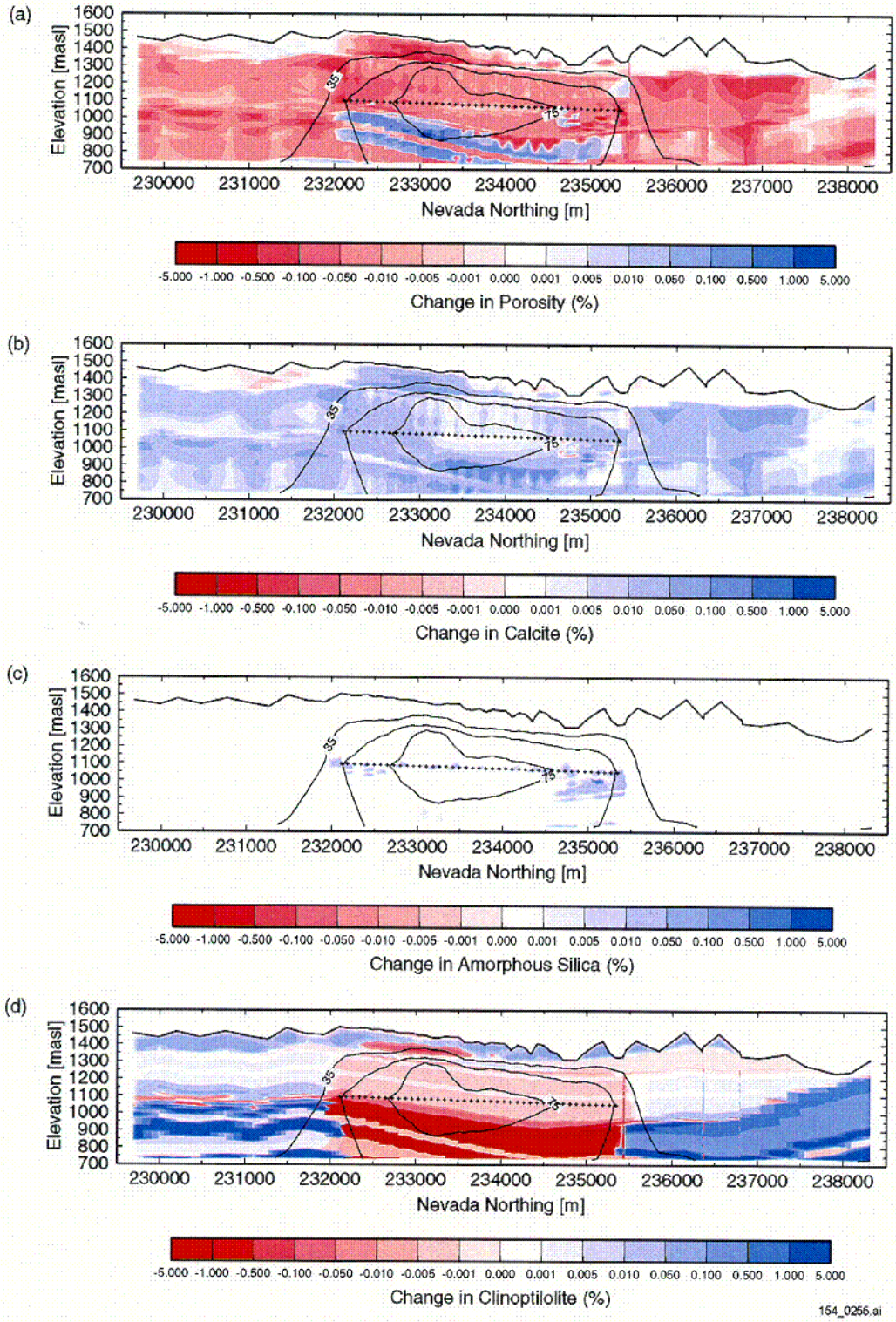

154_0255.ai

Source: Bodvarsson 2001 [DIRS 154669], Attachment 10, pp. 15 to 16.

NOTE: Extended Case 2. Crosses denote model repository drift locations: (a) fracture porosity change with temperature contours; (b) fracture calcite change with temperature contours; (c) fracture amorphous silica precipitation with temperature contours; and (d) matrix clinoptilolite change with temperature contours. masl = meters above sea level.

Figure 3.3.6-4. Simulated Changes in Fracture Porosity and Mineralogy after 5,000 Years of Heating

C37

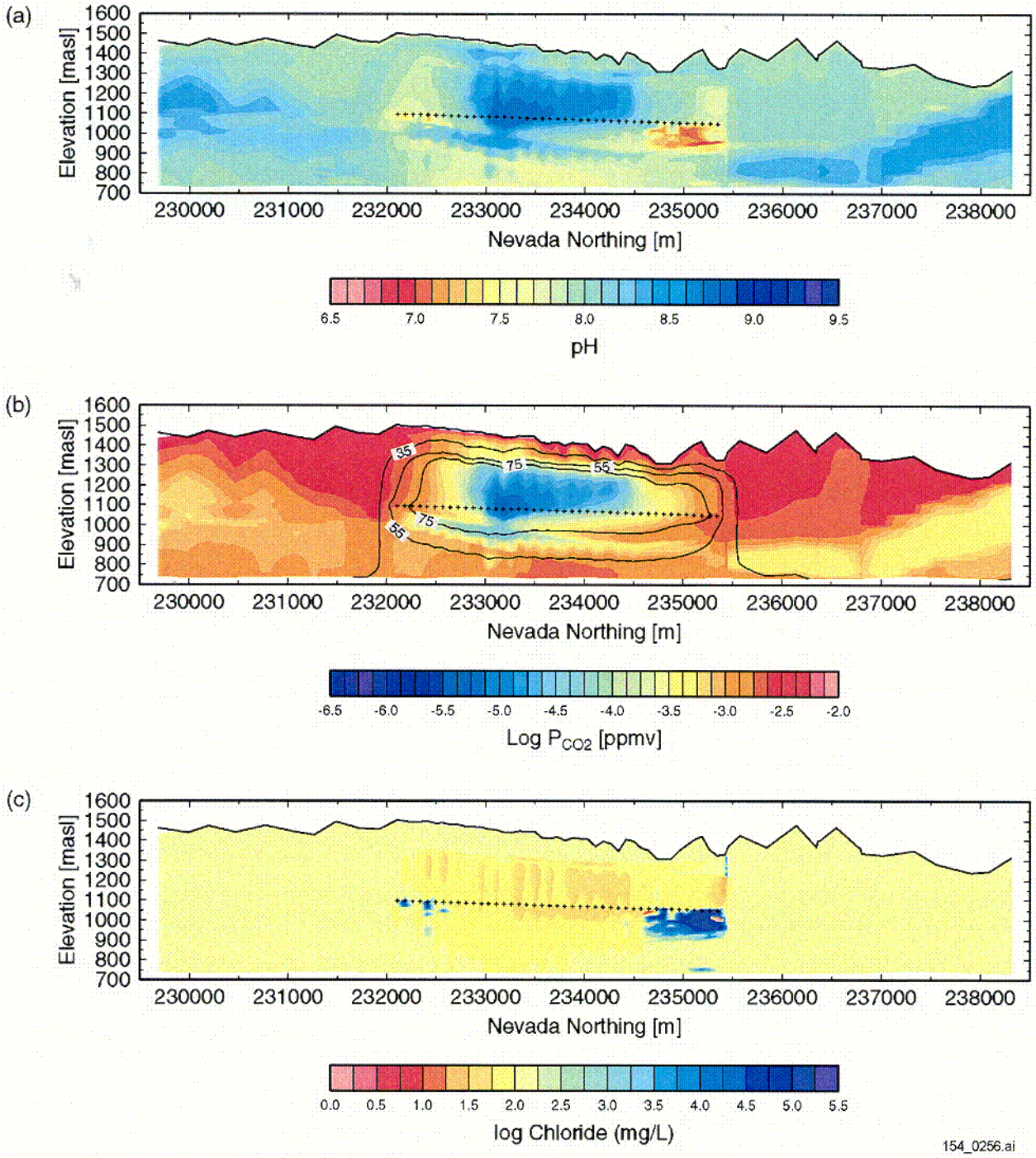

154_0256.ai

Source: Bodvarsson 2001 [DIRS 154669], Attachment 10, pp. 17 to 18.

NOTE: Extended Case 1. Crosses denote model repository drift locations: (a) pH of fracture water; (b) carbon dioxide concentration in gas in fractures with temperature contours; and (c) chloride concentration in fractures. masl = meters above sea level.

Figure 3.3.6-5. Simulated Water and Gas Chemistry after about 1,400 Years of Heating

C38

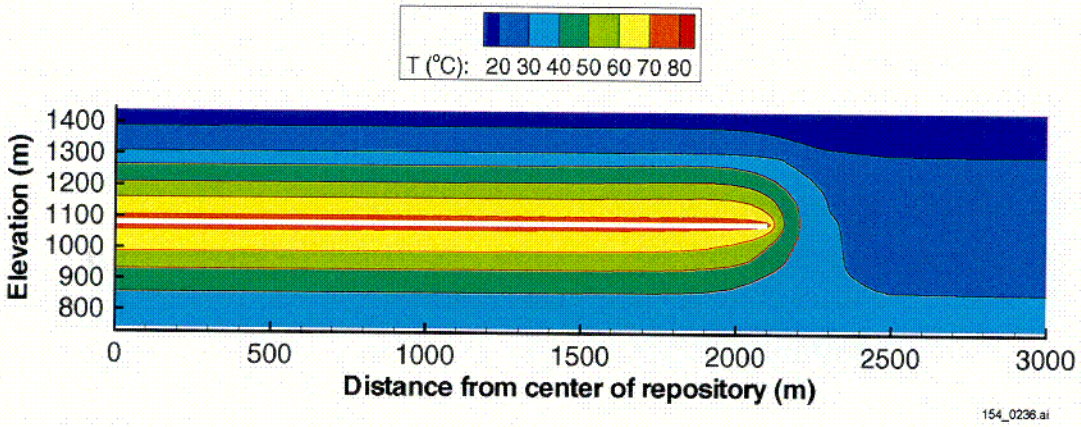

154_0236.ai

Source: Derived from Bodvarsson 2001 [DIRS 154669], Attachment 9, pp. 75 to 78.

Figure 3.3.7-1. Temperature Distribution at 1,000 Years

C39

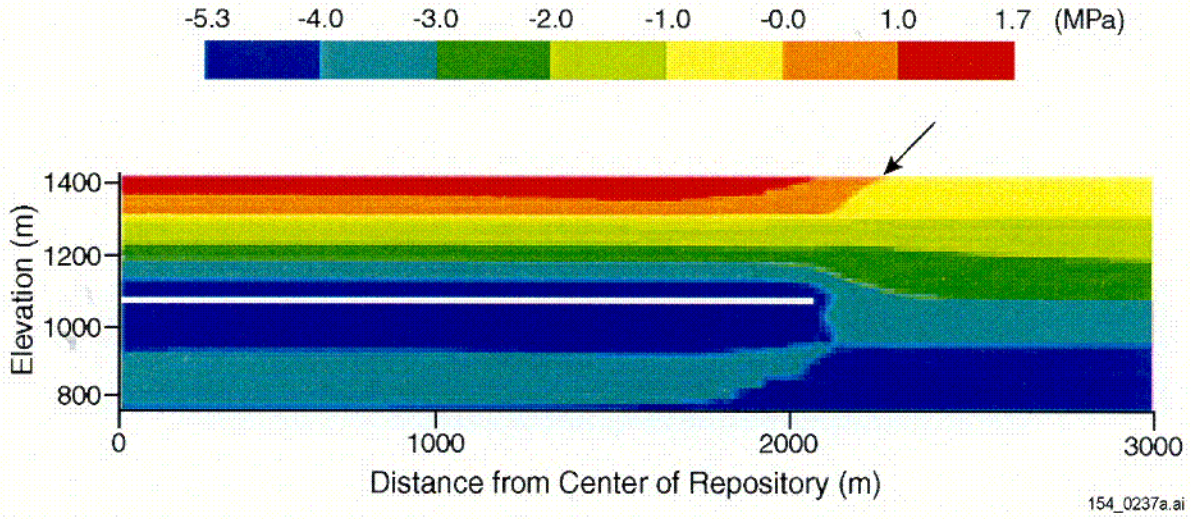

154_0237a.ai

Source: Derived from Bodvarsson 2001 [DIRS 154669], Attachment 9, pp. 75 to 78.

NOTE: Arrow points to contour that separates positive and negative stress values.

Figure 3.3.7-2. Contour of Horizontal Stress Distribution at 1,000 Years

C40

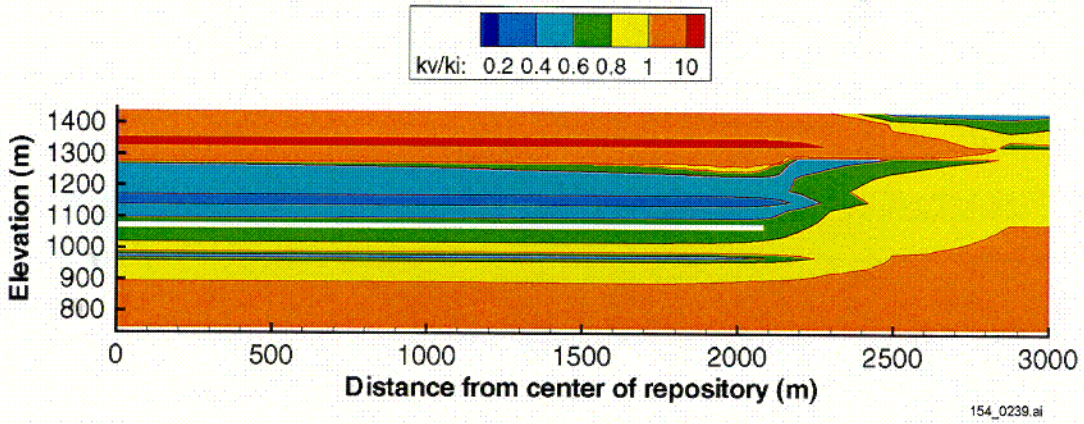

154_0239.ai

Source: Derived from Bodvarsson 2001 [DIRS 154669], Attachment 9, pp. 75 to 78.

Figure 3.3.7-3. Vertical Permeability Changes due to the Thermal-Hydrologic-Mechanical Effect at 1,000 Years

C41

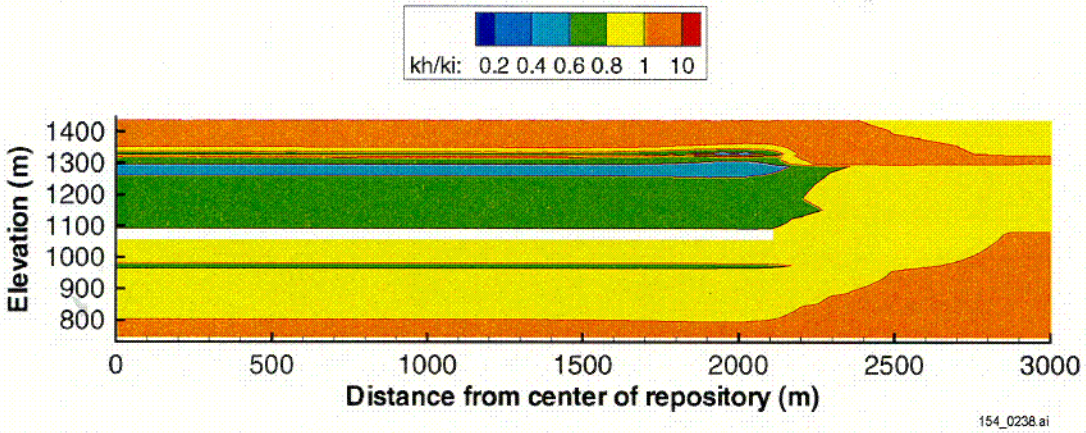

154_0238.ai

Source: Derived from Bodvarsson 2001 [DIRS 154669], Attachment 9, pp. 75 to 78.

Figure 3.3.7-4. Change in Horizontal Permeability Due to the Thermal-Hydrologic-Mechanical Effect at 1,000 Years

C42

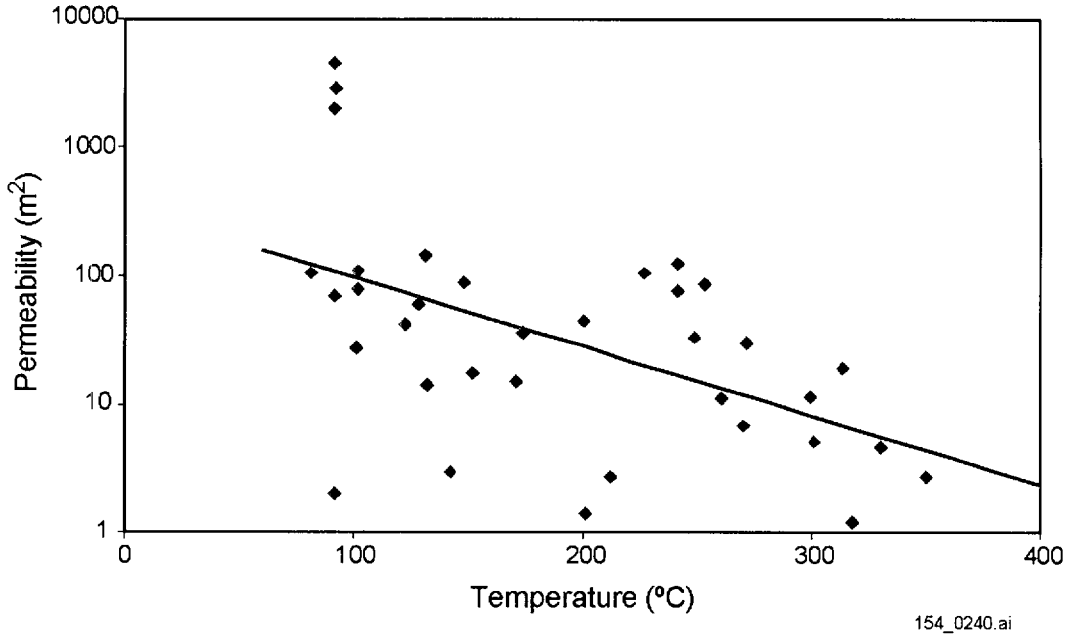

154_0240.ai

NOTE: Based on Figure 1 of Björnsson and Bodvarsson 1990 [DIRS 154606].

Figure 3.3.7-5. Correlation Between Permeability and Temperature of Geothermal Reservoirs Worldwide